AN EFFICIENT METHOD FOR THE SOLUTION OF THE ENERGY DEPENDENT INTEGRAL BOLTZMANN TRANSPORT EQUATION IN THE RESOLVED RESONANCE ENERGY REGION

by

George Arthur Schwenk, Jr.

Dissertation submitted to the Graduate Faculty of the
Virginia Polytechnic Institute and State University
in partial fulfillment of the requirements for the degree of

DOCTOR OF PHILOSOPHY

in

Nuclear Science and Engineering

APPROVED:

M. C. Edlund, Chairman

R. J. Cnega

J. R. Thomas

L. W. Johnson

T. F. Parkinson

March, 1980

Blacksburg, Virginia

ACKNOWLEDGMENTS

Much of this work was performed under research projects funded by Combustion Engineering and Argonne National Laboratory. I am thankful for having the opportunity to work in these projects.

I would like to express my appreciation to all members of my committee for their help and to the Babcock & Wilcox Company for financial assistance.

Special thanks is given to Prof. M. C. Edlund for his advice and guidance.

Finally, I would like to thank my wife, , for enduring many nights at home alone while I worked on this project.

CONTENTS

LIST OF TABLES

LIST OF TABLES (CONT'D)

LIST OF TABLES (CONT'D)

LIST OF FIGURES

1. INTRODUCTION

1.1. Description of Problem and Summary of Solution

The goal of this research is to develop an efficient and accurate method for the calculation of resolved resonance energy region few group cross sections for use in reactor design. The primary motivation for this development is the fact that the MUFT[6] type fast spectrum calculations, which are widely used in the design of current light water reactors, yield considerable errors in k_∞ and conversion ratio [14] for advanced fuel lattice configurations. Among these are the high conversion lattices, proposed by Edlund, [1] which require very accurate calculation of reaction rates in the resolved resonance energy region. For these tight lattices the neutron multiplication factor is much more sensitive to resonance energy region cross sections than conventional fuel lattices currently used in commercial water reactors since a larger fraction of the neutron production occurs in this energy region. The percentage of neutrons produced by fissions occurring in the energy range of 0.625 ev - 5531 ev is approximately 11% in a current light water reactor. This amount increases to about 50% for an advanced high conversion reactor fuel lattice with a fuel to moderator ratio of two to one. About 70% of the neutron absorption occurs below 0.625 ev in current reactor fuel lattices while about 17% occurs below 0.625 ev in a tight lattice.

A review of current reactor design methods shows that a great need exists for the development of an efficient method for the solution of the energy dependent integral Boltzmann transport equation in the resolved resonance energy region. A method is required which could be used by nuclear reactor fuel cycle designers on a production basis. This method should produce accurate results when compared to a reference solution such as the continuous energy Monte Carlo solution calculated by the computer code VIM,[4] which is used as a reference for this study. MUFT-type reactor design codes such as NULIF[2] and CEPAK[3], which utilize the narrow resonance escape probabilities, are fast, yet lack the desired accuracy.

Codes such as RABBLE,[5] STRIP,[10] and MC^2 [28], which perform direct numerical integrations of the Boltzmann Equation with ultra-fine lethargy groups (.0001), are accurate, but are prohibitively expensive for use on a production basis.

A method for obtaining the conflicting goals of efficiency and accuracy is presented in this dissertation. A very efficient multigroup solution of the energy-dependent integral transport equation is derived in Section 2.2. This solution uses an analytical solution of the energy-dependent neutron flux derived in Section 2.4 to obtain flux weighted multigroup cross sections. The use of this analytical flux shape to account for the rapidly varying fine structure of the resonance cross sections allows the multigroup lethargy widths chosen for the numerical integration of the Boltzmann Equation to be

much wider than the group widths used in the direct numerical integration codes. The method developed in this dissertation is called the Broad Group Integral Method (BGIM) for this reason. The use of these broad groups, which are a factor of thirty larger than the groups used in the direct numerical integration procedure, is the key to the BGIM efficiency. It is estimated that for a 10-step unit cell fuel cycle depletion calculation, the computer running time for a unit cell depletion code such as EPRI-LEOPARD[18] would be increased by only 6% if its lower resolved resonance region (1.855 ev - 167 ev) calculation is replaced by the more accurate and intricate BGIM method.

A comprehensive numerical verification of the BGIM method is given in Chapter 3 of this dissertation. Numerous comparisons are made to VIM results for an infinite repeating lattice. The comparisons consider isotopic changes caused by burnup and enrichment variations, cold and hot temperatures in fuel and moderator, and lattice geometry variations. These results show that the Broad Group Integral Method is an efficient and accurate theory for the calculation of neutron-nuclei reaction rates in the lower resolved resonance energy region.

1.2. Discussion of Methods in Use Today

This section gives references for some of the methods for the calculation of resonance energy region few group cross sections that are currently used in PWR core design. A brief outline is given of two industry production codes, NULIF[2] and CEPAK.[3] Some comments are given on benchmark tools such as the Monte Carlo code

VIM[4] and the direct integral method codes like RABBLE.[5]

NULIF and CEPAK use a MUFT[6] type solution for neutron slowing down. The resonance absorption calculation in these codes requires a resonance escape probability for each resonance. NULIF uses either the narrow or wide resonance approximation[25] as appropriate to calculate the resonance escape probability. CEPAK uses the intermediate resonance approximation[7] for the plutonium isotopes and the ω-search[8] method for U-238. Both codes use Dancoff corrections to account for spatial self-shielding.

The NULIF and CEPAK calculations treat each resonance as isolated and do not provide for the ordering of resonances within a micro-group. Therefore, the effects of resonance overlap and interference are neglected and the flux is assumed to have regained its asymptotic value at the beginning of each resonance. These approximations are more appropriate for loose lattices than tight lattices because in the loose lattice we have a greater amount of hydrogen scattering.

Direct integral methods pioneered by Nordheim[9] are used by the codes STRIP[10] and RABBLE. When no approximations are made to the moderator integral, the accuracy of these calculations for homogeneous mixtures is very good and is mainly a function of the integration step size. For the heterogeneous calculation, STRIP treats the cell as a two-region problem of arbitrary geometry. RABBLE cylindrisizes the cell and then performs a multi-region calculation.

Monte Carlo methods such as those used in the code VIM are theoretically the most accurate. The errors in a Monte Carlo calculation are statistical in nature and can be made as small as desired by tracking enough neutron histories. For these reasons the results from the VIM calculations made during this research are treated as benchmark values for the determination of the accuracy of a given method.

Production methods such as those used by NULIF and CEPAK have the advantage of being extremely fast running calculations on a modern digital computer, but their accuracy for tight lattices is questionable (see Section 1.4). Monte Carlo and detailed direct integral methods are accurate but their computer running times (particularly for Monte Carlo) are impractical for use as a production method.

1.3. Description of VIM Code

VIM is a continuous energy Monte Carlo code featuring a versatile geometric capability, and a detailed representation of neutron physics. The development of VIM was initiated at Atomics International[11] and has been continued at Argonne National Laboratory.

VIM contains the combinatorial geometry package developed for the code SAM-CE,[12] which has been extended to include the description of repeating rectangular and hexagonal lattices. The use of combinatorial geometry permits a detailed description of complicated and irregular assemblies. An infinite, homogeneous medium option is also available to provide an efficient capability for data testing

and cross section evaluation.

Cross section definition in VIM is by composition-independent microscopic data sets. Resonance and smooth cross sections are specified pointwise with linear interpolation to provide a continuous energy cross section description; unresolved resonances are described by the probability table method.[13] The reaction types fission, elastic scattering, discrete level inelastic scattering, inelastic continuum scattering, and (n,2n) reaction are specifically defined, while "capture" is defined as the remaining possible outcome of a neutron collision. Neutron trajectories and scattering are continuous in angle. Anisotropic elastic and discrete level inelastic scattering are described with probability tables derived from ENDF/B data. For those materials with thermal scattering law data specified in ENDF/B, the data are run through a series of processing into a code to create the final library of thermal scattering probability tables and thermal inelastic cross sections which is used by VIM. A discussion of the techniques used to generate the VIM cross sections may be found in Refs. 22 and 23.

An independent check of VIM resonance region cross sections was performed at VPI&SU by numerically integrating the data on the VIM cross section library to obtain infinitely dilute resonance integrals for the principal isotopes. These integrals are compared with experimental values in Table 1. The good agreement shown here verifies the VIM data base for these isotopes.

TABLE 1

A Comparison of VIM Calculated and Experimentally Measured Resonance Integrals

Isotope	Calculated Capture Integral (barns)	Calculated Fission Integral (barns)	Measured Capture Integral (barns)	Measured Fission Integral (b
U235*	125	206	128 ± 5	208 ± 10
U238**	286	-	286 ± 8	-
Pu239*	167	215	167 ± 7	231 ± 14

* U235 and Pu239 measured values are above 3 ev and are taken from Reference 26.

** U238 measured value is above .5 ev and is taken from Reference 27.

The VIM code calculates eigenvalues by analog, collision, and track length estimation, and averaging of the various eigenvalue estimates is provided for variance reduction. Both collision and track length estimation are used to provide reaction rate estimates by region, group and isotope, while group and region integrated fluxes are given by track length estimation. Track length estimation of reaction rates and fluxes is used to provide estimates of microscopic cross sections over tally regions. A service code called RETALLY can be used to collapse these tally regions in space and energy as desired to provide things such as cell averaged few group cross sections.

An additional feature of VIM is a user-oriented fixed source option which allows the user to specify the neutron source distribution in space and energy through use of an input FORTRAN subroutine. This option is used to calculate the escape probabilities given in Section 3.7.

1.4. Groundwork

A detailed comparison of the results from the production codes CEPAK and VIM was performed and reported in detail in Reference 14.

Results of the CEPAK and VIM comparison are summarized in Table 2. Detailed comparisons of neutron fluxes, reaction rates and four group microscopic and macroscopic cross sections are presented in Reference 14. Two important findings of this research are:
1) In general, there is very good agreement between CEPAC and VIM on the global quantities, k_∞ and CR (conversion ratio), for the Combustion Engineering system 80 lattice. However, for the tight lattice, considerable difference in k_∞ and CR are noted.
2) In both types of lattices, CEPAK and VIM give reasonably good agreement for the first two neutron groups (0.821 - 10 Mev and 5.53 - 821 Kev). In the resonance group (0.625 ev - 5.53 Kev), however, the CEPAC computation gives more resonance absorption in fissile isotopes than VIM for all cases and therefore a smaller fraction of neutrons are thermalized. These differences increase as the neutron spectrum is hardened and are quite large for the tight lattices - about 20% in the slowing down density into the thermal group.

A comparison between the results of NULIF and VIM was also performed in order to gain better insight into the problem of analyzing tight lattices. This comparison consisted of a heterogeneous and homogeneous calculation of a mixed-oxide fueled, infinite repeating lattice with a fuel to moderator ratio of two to one. The principal

Table 2

COMPARISON OF CEPAC AND VIM RESULTS

Case	%D_2O	Lattice	Fuel	k		CR	
				CEPAC	VIM	CEPAC	VIM
1a	0	C-E*	3 w/o U-235 97 w/o U-238	1.210	1.205	0.405	0.410
1b	50	C-E	4 w/o U-235 16 w/o U-238 80 w/o Th-232	1.210	1.208	0.559	0.572
1c	50	C-E	4.46 w/o Pu in Th-232	1.175	1.171	0.597	0.599
1d	0	C-E	1.95 w/o U-233 in U-238	1.425	1.422	0.498	0.499
2a	50	T-L**	4.2 w/o U-233 in U-238	1.176	1.226	0.896	0.818
2c	0	T-L	7.34 w/o Pu in U-238	1.182	1.154	0.768	0.781

* Standard C-E Lattice - Fuel/Water = 0.585

** Tight Lattice - Fuel/Water = 1.96

CR = Conversion Ratio

results from these calculations are summarized in Tables 3 and 4.

Two important indications were obtained from this comparison. First, since the differences between the two codes were approximately the same in both the homogeneous and heterogeneous calculation, the major problem with the tight lattice calculation lies in the energy solution, rather than with the intra-cell spatial calculation. Second, as can be seen in the differences in the microscopic cross sections in Table 3 and the absorption rates in Table 4, the major problem is in the lower resolved resonance energy range.

TABLE 3

COMPARISON OF VIM AND NULIF FOR A CLOSE PACKED PU-U LATTICE-MICROSCOPIC CROSS SECTIONS

HOMOGENEOUS CELL

Code	K_∞	σ_a^{239*} (barns)	σ_a^{238**} (barns)
NULIF	1.124	70.30	3.510
VIM	1.094	60.18	4.163
% DEVIATION	(.4)**	(1.09)	(1.11)

HETEROGENEOUS CELL

NULIF	1.182	65.76	3.140
VIM	1.154	53.39	3.407
% DEVIATION	(0.4)	(1.76)	(2.62)

* Cross Sections are averaged over the energy range 1.855 ev - 61 ev

** % Deviation - 1 standard deviation

TABLE 4

COMPARISON OF VIM AND NULIF FOR A CLOSE PACKED PU-U LATTICE-ABSORPTION RATES

E Lower (ev)	VIM Absorption Rate*	NULIF Absorption Rate
3355	.01522	.01501
2035	.01819	.01807
1234	.01830	.01943
749	.02490	.02723
454	.02748	.02892
275	.02694	.03020
167	.03918	.04213
101	.04284	.05120
61	.05451	.06996
37	.04748	.06189
23	.03900	.03312
13.7	.06604	.08205
8.3	.03813	.04994
5.0	.06106	.06258
3.1	.01694	.01582
1.9	.02543	.02104
Total	.56164	.62933

* Typical VIM Deviations are 3-5%.

2. METHOD OF SOLUTION

2.1. General Description of the Broad Group Integral Method (BGIM)

The Broad Group Integral Method is a multigroup, integral solution of the Transport Equation in the resolved resonance energy range. The method uses broad multigroups (approximately 0.003 lethargy units) to obtain an efficient solution. The use of these broad groups necessitates the derivation of a special set of multigroup equations which make use of an analytical flux shape to obtain the required integral multigroup parameters. This analytical flux shape is derived directly from the transport equation (Section 2.4) by making some simplifying assumptions.

BGIM is derived assuming an infinite array of identical cells modeled in two spatial regions, typically fuel and moderator. The interaction between regions is determined by escape probabilities which are extensively benchmarked against Monte Carlo results.

BGIM is a very efficient method which allows for explicit treatment of resonance overlap and interference and performs an accurate solution of the spatial problem. BGIM is intended to form the theoretical base for a subroutine in a MUFT-type code which is used in the lower resolved resonance region. This subroutine could be called whenever an accurate solution of the resonance range is needed (e.g. in tight, high-conversion lattices).

2.2. Derivation of Multigroup Equations

This section presents the derivation of a general set of multigroup equations, governing neutron transport in the lower resolved resonance region, that can be solved rapidly on a digital computer. These equations are derived with a constraint requiring a lethargy group width less than the maximum lethargy gain in a collision with the heaviest isotope in the problem. However, the equations are derived with the idea that the group width will be chosen as large as possible within this constraint in order to obtain the most efficient solution.

The derivation begins with the energy-dependent steady-state neutron continuity equation (2.2.1) in the resolved resonance energy region specialized to a two-region cell of fuel (f) and moderator (m).

$$\nabla \cdot J(r,E) + \Sigma_{t_{(m)}}(E)\phi(r,E) = \int_0^\infty \Sigma_{s_{(m)}}(E' \to E)\phi(r,E')dE' \qquad \text{for } r \text{ in } V_m$$

$$\nabla \cdot J(r,E) + \Sigma_{t_{(f)}}(E)\phi(r,E) = \int_0^\infty \Sigma_{s_{(f)}}(E' \to E)\phi(r,E')dE' \qquad \text{for } r \text{ in } V_f \qquad (2.2.1)$$

Integrating these equations over V_m and V_f respectively and making use of Gauss's Theorem and definitions (2.2.2), Eqs. (2.2.3) are obtained, where n_m and n_f are unit vectors drawn outward perpendicular to the surface.

$$\bar{\phi}^m(E) \equiv \frac{\int_{V_m} \phi(r,E)dV}{V_m}$$

$$\bar{\phi}^f(E) \equiv \frac{\int_{V_f} \phi(r,E)dV}{V_f} \qquad (2.2.2)$$

$$\int_{S_m} J(r,E) \cdot n_m dS + \Sigma_{t_{(m)}}(E)V_m\bar{\phi}^m(E) = V_m \int_o^\infty \Sigma_{S_{(m)}}(E'\to E)\bar{\phi}^m(E')dE'$$

(2.2.3)

$$\int_{S_f} J(r,E) \cdot n_f dS + \Sigma_{t_{(f)}}(E)V_f\bar{\phi}^f(E) = V_f \int_o^\infty \Sigma_{S_{(f)}}(E'\to E)\bar{\phi}^f(E')dE'$$

Assuming that the cell of interest is in an infinite array of like cells causes the net leakage across the outer boundary of the cell to equal zero. Hence, the net leakage out of V_m is equal and opposite to the net leakage out of V_f, which is stated mathematically in Eq. (2.2.4):

$$\int_{S_m} J(r,E) \cdot n_m dS = - \int_{S_f} J(r,E) \cdot n_f dS \qquad (2.2.4)$$

Now the flux and current may be split into two parts as follows:

$$\begin{aligned} \phi(r,E) &= \phi_f(r,E) + \phi_m(r,E) \\ J(r,E) &= J_f(r,E) + J_m(r,E) \end{aligned} \qquad (2.2.5)$$

The functions $\phi_f(r,E)$ and $J_f(r,E)$ are the flux and net current densities throughout the lattice due to sources in the fuel rods alone, while $\phi_m(r,E)$ and $J_m(r,E)$ are the flux and net current densities throughout the lattice due to sources in the moderator regions alone. These partial fluxes and currents obey Eq. (2.2.6) where H^f is the Heaviside step function, which is unity in the fuel rod and zero in the moderator, and $H^m = 1 - H^f$.

$$\begin{aligned} \nabla \cdot J_f(r,E) + \Sigma_t(r,E)\phi_f(r,E) &= \int_0^\infty dE' \, \Sigma_{S_{(f)}} (E' \to E)\phi(r,E')H^f \\ \nabla \cdot J_m(r,E) + \Sigma_t(r,E)\phi_m(r,E) &= \int_0^\infty dE' \, \Sigma_{S_{(m)}} (E' \to E)\phi(r,E)H^m \end{aligned} \qquad (2.2.6)$$

Integrating Eq. (2.2.3) over V_f and V_m respectively, applying Gauss's law and definitions (2.2.2) of the region fluxes and (2.2.7) of the escape probabilities and performing some mathematical manipulation, the coupled integral equations (2.2.8) are obtained for $\bar{\phi}^m(E)$ and $\bar{\phi}^f(E)$.

$$P_f(E) \equiv \frac{\Sigma_{t_{(m)}}(E)\, V_m\, \bar{\phi}^m_f(E)}{V_f \int_o^\infty dE'\, \Sigma_{S_{(f)}}(E' \to E)\bar{\phi}^f(E')} \tag{2.2.7}$$

$$P_m(E) \equiv \frac{\Sigma_{t_{(f)}}(E)\, V_f\, \bar{\phi}^f_m(E)}{V_m \int_o^\infty dE'\, \Sigma_{S_{(m)}}(E' \to E)\bar{\phi}^m(E')}$$

$$\Sigma_{t_{(m)}}\bar{\phi}^m(E) = [1 - P_m(E)] \int_o^\infty \Sigma_{S_m}(E' \to E)\bar{\phi}^m(E')dE' + P_f(E)\frac{V_f}{V_m}\int_o^\infty \Sigma_{S_{(f)}}(E' \to E)\bar{\phi}^f(E')dE' \tag{2.2.8}$$

$$\Sigma_{t_{(f)}}(E)\bar{\phi}^f(E) = [1 - P_f(E)] \int_o^\infty \Sigma_{S_{(f)}}(E' \to E)\bar{\phi}^f(E')dE' + P_m(E)\frac{V_m}{V_f}\int_o^\infty \Sigma_{S_{(m)}}(E' \to E)\bar{\phi}^m(E')dE'$$

For computational purposes it is more convenient to work in the lethargy variable (u) so in equations (2.2.10), the energy variable (E) is transformed to u making use of Eq. (2.2.9) for the scattering probability from lethargy u' to u for region i and isotope j. This equation is derived assuming isotropic scattering in the center of mass system. This assumption will be a very good one in the resolved resonance energy range of interest since p-wave (anisotropic in the center of mass system) scattering is very small compared to s-wave scattering below 10 KeV.

$$\Sigma^j_{S(i)}(u' \to u) = \frac{\Sigma^j_{S(i)}(u')_{e^{-\Delta u}}}{(1-\alpha_j)} \qquad \text{for } u \le u' \le u - \epsilon_j$$

$$= 0 \text{ for } u' > 0 \text{ and } u' < u - \epsilon_j \qquad (2.2.9)$$

where $\alpha_j = \frac{(A_j - 1)^2}{(A_j + 1)^2}$; A_j is the atomic weight of isotope j

and ϵ_j is the maximum lethargy gain in a collision with an atom or nucleus of isotope j.

The following set of coupled integral equations in lethargy obtained using these substitutions are similar to those solved by RABBLE[5] and STRIP[10] using direct numerical integration.

$$\Sigma_{t_{(m)}}(u)\bar{\phi}^{m}(u) = [1 - P_m(u)] \sum_j \int_{u-\varepsilon_j}^{u} e^{-(u-u')} \frac{\Sigma^j_{S_{(m)}}(u')\bar{\phi}^{m}(u')du'}{(1-\alpha_j)}$$

$$+ P_f(u) \frac{V_f}{V_m} \sum_j \int_{u-\varepsilon_j}^{u} e^{-(u-u')} \frac{\Sigma^j_{S_f}(u')\bar{\phi}^{f}(u')du'}{(1-\alpha_j)} \qquad (2.2.10)$$

$$\Sigma_{t_{(f)}}(u)\bar{\phi}^{f}(u) = [1 - P_f(u)] \sum_j \int_{u-\varepsilon_j}^{u} e^{-(u-u')} \frac{\Sigma_{S_{(f)}}(u')\bar{\phi}^{f}(u')du'}{(1-\alpha_j)}$$

$$+ P_m(u)\, V_m/V_f \sum_j \int_{u-\varepsilon_j}^{u} e^{-(u-u')} \frac{\Sigma_{S_{(m)}}(u')\bar{\phi}^{m}(u')du'}{(1-\alpha_j)}$$

where $\varepsilon_j = 2 \ln \frac{(A_j + 1)}{(A_j - 1)}$ for j other than hydrogen

$\varepsilon_{hydrogen} = u$

Now make definition (2.2.11) where i denotes the region and j denotes the isotope:

$$S^j_i(u) \equiv \int_{u-\varepsilon_j}^{u} \frac{e^{-(u-u')}\Sigma_{S_{(i)}}(u')\bar{\phi}^{i}(u')du'}{(1-\alpha_j)} \qquad (2.2.11)$$

Physically, $S_i^j(u)$ is the source of neutrons at lethargy u from scattering from isotope j in region i. Making use of definition (2.2.11), Eq. (2.2.10) simplifies to:

$$\Sigma_{t_{(m)}}(u)\bar{\phi}^m(u) = [1 - P_m(u)] \sum_j S_m^j(u) + \frac{V_f}{V_m} P_f(u) \sum_j S_f^j(u)$$

$$\Sigma_{t_{(f)}}(u)\bar{\phi}^f(u) = [1 - P_f(u)] \sum_j S_f^j(u) + V_m/V_f \, P_m(u) \sum_j S_m^j(u) \qquad (2.2.12)$$

The integral multigroup equations (2.2.15) are obtained by integrating Eq. (2.2.12) from u_{n-1} to u_n, which is an arbitrary multigroup denoted the n^{th} group, and by making use of definitions of the following definitions:

$$\Sigma_{x_n}^i \equiv \frac{\int_{u_{n-1}}^{u_n} \Sigma_x(u)\bar{\phi}^i(u)du}{\int_{u_{n-1}}^{u_n} \bar{\phi}^i(u)du} \qquad (2.2.13)$$

$$\bar{\phi}_n^i \equiv \frac{\int_{u_{n-1}}^{u_n} \bar{\phi}^i(u)du}{\int_{u_{n-1}}^{u_n} du} = \frac{\int_{u_{n-1}}^{u_n} \bar{\phi}^i(u)du}{\Delta_n} \qquad (2.2.14)$$

where x denotes type of cross section, e.g., t, f, c, s (total, fission, capture, elastic scattering).

$$\Delta_n \Sigma_{t_n}^m \bar{\phi}_n^m = \int_{u_{n-1}}^{u_n} [(1 - P_m(u)) \sum_j S_m^j(u) + \frac{V_f}{V_m} P_f(u) \sum_j S_f^j(u)]du \tag{2.2.15}$$

$$\Delta_n \Sigma_{t_n}^f \bar{\phi}_n^f = \int_{u_{n-1}}^{u_n} [(1 - P_f(u)) \sum_j S_f^j(u) + \frac{V_m}{V_f} P_m(u) \sum_j S_m^j(u)]du$$

In order to perform the integrations on the right-hand side of Eq. (2.2.15), $S_i^j(u)$ is first examined for isotopes j other than hydrogen. Expressing the integral in (2.2.15) as a sum of integrals over multigroups and making use of definition (2.2.16), Eq. (2.2.17) is obtained for $S_i^j(u)$.

$$K_i^j(u') \equiv \frac{e^{u'} \Sigma_{S_{(i)}}^j(u') \bar{\phi}^i(u')}{(1 - \alpha_j)} \tag{2.2.16}$$

$$S_i^j(u) = e^{-u}[\int_{u-\epsilon_j}^{u_n - L_j - 1} K_i^j(u')du' + \sum_{\ell=1}^{L_j} \int_{u_{n-\ell-1}}^{u_{n-\ell}} K_i^j(u')du' \tag{2.2.17}$$

$$+ \int_{u_{n-1}}^{u} K_i^j(u')du'] \quad \text{for } u_{n-1} \leq u \leq u_n$$

where L_j is the maximum number of lethargy groups that a neutron can

scatter through and arrive at u_n. Making the following definitions an equation for $S_i^j(u)$ is obtained:

$$K_{i_n}^j \equiv \frac{\int_{u_{n-1}}^{u_n} K_i^j(u')du'}{\int_{u_{n-1}}^{u_n} \bar{\phi}^{-1}(u')du'} \qquad (2.2.18)$$

$$SUM_{i_n}^j \equiv \sum_{\ell=1}^{L_j} K_{i_{n-\ell}}^j \bar{\phi}_{n-\ell}^{-1} \Delta_{n-\ell} \qquad (2.2.19)$$

$$S_i^j(u) = e^{-u} \left[\int_{u-\varepsilon_j}^{u_n-L_j-1} K_i^j(u')du' + SUM_{i_n}^j \right. \qquad (2.2.20)$$

$$\left. + \int_{u_{n-1}}^{u} K_i^j(u')du' \right] \text{ for } u_{n-1} \le u \le u$$

It is now realized, examining Eq. (2.2.20), that during the numerical solution of the multigroup equations, $SUM_{i_n}^j$ will be a sum of products of previously determined multigroup parameters and fluxes. Therefore, the difficulty in obtaining $S_i^j(u)$ lies in the evaluation of the first and the third terms in the brackets in Eq. (2.2.20).

Making definition (2.2.21) the first term of Eq. (2.2.20) will become $R_1^j(u)\, K^j_{i_{n-L_j-1}} \bar{\phi}^i_{n-L_j-1} \Delta_{n-L_j-1}$ and since $K^j_{i_{n-L_j-1}}$, $\bar{\phi}^i_{n-L_j-1}$, Δ_{n-L_j-1} are previously determined parameters, the task of evaluating the first term of Eq. (2.2.20) is reduced to the evaluation of $R_1^j(u)$.

$$R_1^j(u) \equiv \frac{\int_{u-\epsilon_j}^{u_{n-L_j-1}} K_1^j(u')du'}{\int_{u_{n-L_j-2}}^{u_{n-L_j-1}} K_1^j(u')du'} \qquad \text{for } u_{n-1} \le u \le u_n \tag{2.2.21}$$

The evaluation of $R_1^j(u)$ will be performed by assuming that $\Sigma^j_{S_i}(u)\, \bar{\phi}^i(u')$ is constant over the ranges of integration in (2.2.21). This assumption will be accurate since the multigroup width will be chosen narrow enough so that the variation of $\Sigma^j_{S_i}(u')\bar{\phi}^i(u')$ will be small and the contribution of the first term of Eq. (2.2.20) will be much smaller than $SUM^j_{i_n}$. Making this assumption, the evaluation of $R_1^j(u)$ requires only the integration of simple exponentials to yield

$$R_1^j(u) = \exp(u_{n-L_j-1} + \epsilon_j - \Delta_{n-L_j-1} - u) \tag{2.2.22}$$

The evaluation of the third term in Eq. (2.2.20) is done by making definition (2.2.23) for $Z_1^j(u)$ and following the same derivation for $Z_1^j(u)$ as for $R_1^j(u)$ to obtain Eq. (2.2.24).

$$Z_1^j(u) \equiv \frac{\int_{u_{n-1}}^{u} K_1^j(u')du'}{\int_{u_{n-1}}^{u_n} K_1^j(u')du'} \qquad (2.2.23)$$

$$Z_1^j(u) = \exp(u - u_{n-1} - \Delta_n) \qquad (2.2.24)$$

So finally $S_1^j(u)$ can be written as follows:

$$S_1^j(u) = e^{-u}[R_1^j(u)\, K^j_{1_{n-L_j-1}} \bar{\phi}_{n-L_j-1} \Delta_{n-L_j-1} + SUM^j_{1_n}$$

$$+ Z_1^j(u)\, K^j_{1_n} \bar{\phi}^1_n \Delta_n] \qquad (2.2.25)$$

where $R_1^j(u)$ and $Z_1^j(u)$ are evaluated by equations (2.2.23) and (2.2.24) respectively.

The derivation of the multigroup equations up to this point has been quite general, allowing for an arbitrary lethargy group width. However, since the total number of groups will be relatively small (the computer time gains from unequal groups will be small) and since the form of the equations will be greatly simplified by requiring constant width lethargy groups, this requirement is now introduced. Requiring equal lethargy width groups allows $R_1^j(u)$ and $Z_1^j(u)$ to be simplified to the exponential functions given in equations (2.2.26) and (2.2.27), where the superscripts and subscripts for R(u) and Z(u) are dropped since these functions are now independent of isotope and region.

$$R(u) = \exp(u_n - u - \Delta) \tag{2.2.26}$$

$$Z(u) = \exp(u - u_n) \tag{2.2.27}$$

Now Eq. (2.2.25) becomes

$$S_i^j(u) = e^{-u}[\exp(u_n - u - \Delta)\, K_{i\,n-L_j-1}^{j}\, \bar{\phi}_{n-L_j-1}^{i}\, \Delta + SUM_{i\,n}^{j} + \exp(u - u_n)\, K_{i\,n}^{j}\, \bar{\phi}_n^i\, \Delta] \tag{2.2.28}$$

Figure 1 illustrates the relative positions of the various lethargy variables in lethargy space. The ranges of integration for the primed variables are also shown. Integration of the primed variables is necessary to obtain the functions of the unprimed lethargy variable Z(u), R(u), and the K functions which are needed to obtain SUM. The primed variables have been subscripted for identification. The variables u'_Z, u'_R and u'_S are integrated to obtain Z(u), R(u) and the terms of SUM respectively.

Typical lethargy deltas for the integration step size, the multigroup widths and the maximum lethargy gained in a collision with the heaviest isotope are given. These values show the basis for the name BGIM. The multigroups (0.003) are broad with respect to typical group widths (0.0001) that are used in the integral method codes STRIP and RABBLE. It should be noted that these groups are narrow relative to MUFT microgroups and the maximum lethargy gained in a collision with the heaviest isotope.

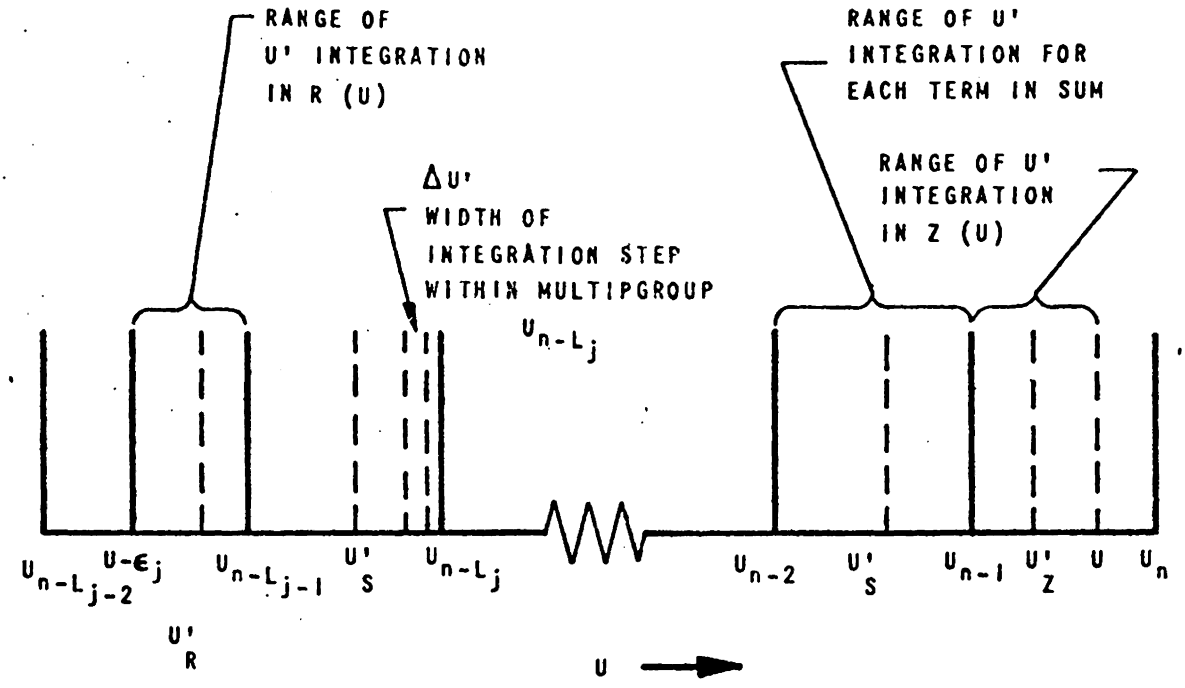

TYPICAL LETHARGY WIDTHS:

$U_n - U_{n-1}$ (STRIP & RABBLE)	=	.0001
$\Delta U'$	=	.00015
$U_n - U_{n-1}$	=	.003
$U - (U - \epsilon_j)$	=	.017
MICROGROUP (MUFT)	=	.25

Figure 1 LETHARGY VARIABLE DIAGRAM AND TYPICAL LETHARGY WIDTHS

Eq. (2.2.28) gives the source of neutrons at lethargy u due to scattering off isotopes j other than hydrogen in region i. Returning to definition (2.2.11), it can be seen that the source due to hydrogen in the moderator is given by

$$S_m^H(u) = \int_o^u e^{-(u-u')} \Sigma_{S(m)}^H(u')\bar{\phi}^m(u')du' \qquad (2.2.29)$$

Finally, substituting equations (2.2.28) and (2.2.29) for the sources into the balance equations (2.2.15), equations (2.2.30) are obtained. The order of the summations and the integrations are switched and those terms independent of u are removed from under the integral sign. Also, $S_m^H(u)$ is assumed constant between u_{n-1} and u_n and equal to $S_{m_n}^H$.

$$\Delta \Sigma_{t_n}^m \bar{\phi}_n^m = \sum_{j\neq H} [e^{u_{n-1}} K_{m_{n-L_j-1}}^j \bar{\phi}_{n-L_j-1}^m \Delta(\int_{u_{n-1}}^{u_n} e^{-2u}du - \int_{u_{n-1}}^{u_n} P_m(u)e^{-2u}du)$$

$$+ SUM_{m_n}^j (\int_{u_{n-1}}^{u_n} e^{-u}du - \int_{u_{n-1}}^{u_n} P_m(u)e^{-u}du)$$

$$+ e^{-u_n} K_{m_n}^j \bar{\phi}_n^m \Delta(\int_{u_{n-1}}^{u_n} du - \int_{u_{n-1}}^{u_n} P_m(u)du)$$

$$+ \frac{V_f}{V_m} [e^{u_{n-1}} K_{f_{n-L_j-1}}^j \bar{\phi}_{n-L_j-1}^f \Delta(\int_{u_{n-1}}^{u_n} e^{-2u} P_f(u)du)$$

$$+ SUM_{f_n}^j (\int_{u_{n-1}}^{u_n} P_f(u)e^{-u}du) + K_{f_n}^j \bar{\phi}_n^f \Delta e^{-u_n}(\int_{u_{n-1}}^{u_n} P_f(u)du)]$$

$$+ S_{m_n}^H (\int_{u_{n-1}}^{u_n} du - \int_{u_{n-1}}^{u_n} P_m(u)du) \qquad (2.2.30A)$$

$$\Delta \Sigma^{f}_{t_n} \bar{\phi}^{f}_{n} = \sum_{j \neq H} [e^{u_{n-1}} K^{j}_{f_{n-L_j-1}} \bar{\phi}_{n-L_j-1} \Delta$$

$$\left(\int_{u_{n-1}}^{u_n} e^{-2u} du - \int_{u_{n-1}}^{u_n} P_f(u)\, e^{-2u} du\right)$$

$$+ \; SUM^{j}_{f_n} \left(\int_{u_{n-1}}^{u_n} e^{-u} du - \int_{u_{n-1}}^{u_n} P_f(u)\, e^{-u} du\right)$$

$$+ \; e^{-u_n} K^{j}_{f_n} \bar{\phi}^{f}_{n} \Delta\left(\int_{u_{n-1}}^{u_n} du - \int_{u_{n-1}}^{u_n} P_f(u) du\right) + \qquad (2.2.30B)$$

$$\frac{V_m}{V_f} [e^{u_{n-1}} K^{j}_{m_{n-L_j-1}} \bar{\phi}^{f}_{n-L_j-1} \Delta\left(\int_{u_{n-1}}^{u_n} e^{-2u} P_m(u) du\right) +$$

$$SUM^{j}_{m_n} \left(\int_{u_{n-1}}^{u_n} e^{-u} P_m(u) du\right) + e^{-u_n} \Delta K^{j}_{m_n} \bar{\phi}^{m}_{n} \int_{u_{n-1}}^{u_n} P_m(u) du]]$$

$$+ \; \frac{V_m}{V_f} S^{H}_{m_n} \int_{u_{n-1}}^{u_n} P_m(u) du$$

Eqs. (2.2.30) are the key coupled equations which are solved by BGIM to obtain the multigroup fluxes in the fuel and moderator.

Eq. (2.2.30) can now be solved efficiently on a digital computer using a stepping up in lethargy process starting from some initial value of u provided the following tasks are accomplished.

1. Develop a fast and accurate method for the calculation of $P_m(u)$ and $P_f(u)$.

2. Derive a simple analytic expression for the shape of the flux within a multigroup n which would be used to calculate $\Sigma^i_{t_n}$, $K^j_{i_n}$ and the microscopic total, fission and scattering multigroup cross sections.

3. Determine the starting values for $SUM^j_{i_n}$ and $S^H_{m_n}$ and develop efficient recurrence relationships for determining $SUM^j_{i_{n+1}}$ and $S^H_{m_{n+1}}$.

The first of these tasks is investigated in section (2.3) the second in section (2.4) and the third in section (2.5).

2.3. Theoretical Discussion of Escape Probabilities

The general forms for the escape probabilities from fuel and moderator are given in Eq. (2.3.1) and Eq. (2.3.2) respectively.

$$P_f(E) = \frac{\Sigma_{t_{(m)}}(E)\, V_m \bar{\phi}^m_f(E)}{V_f \int_o^\infty dE'\, \Sigma_{S_{(f)}}(E' \to E) \bar{\phi}^f(E')} \tag{2.3.1}$$

$$P_m(E) = \frac{\Sigma_{t_{(f)}}(E)\, V_f\, \bar{\phi}^f_m(E)}{V_m \int_o^\infty dE'\, \Sigma_{S_{(m)}}(E' \to E) \phi^m(E')} \tag{2.3.2}$$

Inspection of the general forms of $P_f(E)$ and $P_m(E)$ shows that in order to calculate these escape probabilities exactly, $\phi_f(\bar{r},E)$ and $\phi_m(\bar{r},E)$ must be determined. This would require the solution of two transport-type equations at all energies and at all positions throughout the cell. In order to avoid this extremely difficult problem the following assumption is made:

$$\int_0^\infty dE' \; \Sigma_{S_f}(E' \to E)\phi(\bar{r},E')H^{(f)} = S_f(E)H^f$$

$$\int_0^\infty dE' \; \Sigma_{S_m}(E' \to E)\phi(\bar{r},E')H^{(m)} = S_m(E)H^{(m)} \qquad (2.3.3)$$

This approximation, which is sometimes called the flat source approximation, is discussed in great detail by Henry[15], Kirby[16] and other authors. The key point is that this assumption decouples the energy and spatial dependencies of the partial fluxes. Therefore, the still very difficult, yet manageable, problem of solving a set of individual spatial equations at different energies is left to be done.

The physical justification for assuming a flat source in the fuel and in the moderator is that most of the neutrons appearing in an energy range dE as a result of scattering from higher energies come from energy ranges outside of resonances. The scattering cross section between resonances is small (approximately 10 barns) and the absorption cross section is essentially zero. This means that the spatial flux shape, even though it is severely perturbed near resonant energies, is fairly flat over most of the energy range of the source integral. Thus assuming that the source integrals themselves are independent of $\bar{r}$ is intuitively a reasonable assumption.

There are additional practical and documented justifications for the use of (2.3.3). From a practical point of view, the flat source approximation is essential to the objective of developing a fast running computer code for the calculation of resonance region reaction rates on a production basis. Furthermore, Kirby[16] documents calculations to determine the validity of the flat source approximation. It is his finding that Eq. (2.3.3), though inexact, yields essentially the same effective capture cross sections in the resolved resonance energy region as those calculated using an exact source distribution.

A very important consequence of the flat source approximation is the following equivalence:

$$P_f(E)V_f\Sigma_{t_{(f)}}(E) = P_m(E)V_m\Sigma_{t_{(m)}}(E) \qquad (2.3.4)$$

This equation is known as the reciprocity relationship. Two slightly different derivations of this relationship are discussed by Henry[15] and Bell[17]. The reciprocity relationship allows the determination of $P_m(E)$ from $P_f(E)$ so the main task is reduced to finding $P_f(E)$.

An exact relationship for $P_f(E)$ for a fuel rod that is part of a lattice is given in reference 15 as follows:

$$P_f(E) = \frac{1}{\bar{\ell}_f\Sigma_{t_{(f)}}(E)} \langle(1 - G_f^1)[1 - G_m^1 + G_m^1G_f^2(1 - G_m^2) + \ldots]\rangle \qquad (2.3.5)$$

where $\bar{\ell}_f$ is the mean chord length in the fuel, and G_f^i, G_m^i are the transmission probabilities for the i^{th} rod and clump of moderator with 1 representing the rod of interest and 2 being the next rod traversed along a given chord. The brackets <> stand for the "Chord-Averaging Operator" given by

$$1/(\pi A)\int_A dA \int_{\bar{\Omega} \cdot \bar{n}_1 > 0} d\bar{\Omega}\bar{n}_1 \cdot \bar{\Omega} \qquad (2.3.6)$$

Eq. (2.3.5) is completely intractable unless the well known Bell approximation is made. The Bell approximation for this complicated average of the product of the attenuation factors G_j^i is made by assuming the average of the product to be the product of the averages. There is no rigorous mathematical derivation of this approximation but comparisons with the exact Monte Carlo results in section (3.7) show it to be a very good one.

The attenuation factors are defined

$$G_i^j(E) \equiv \exp(-\Sigma_{t(i)}(E)\, R_{s_{(i)}}^{(j)}).$$

The subscript (i) indicating fuel material (f) or moderator material (m) and superscript (j) indicating the sequence of distances traversed, with $R_{s_{(i)}}^{(j)}$ standing for the successive distances that a neutron will traverse as it passes through alternate regions of fuel and moderator.

$$P_f(E) \approx \frac{1}{\bar{\ell}_f \Sigma_{t_{(f)}}(E)} \{[1 - \langle G_f \rangle][1 - \langle G_m \rangle + \langle G_m \rangle \langle G_f \rangle$$

$$(1 - \langle G_m \rangle) + \ldots .]$$

$$= \frac{[1 - \langle G_f \rangle][1 - \langle G_m \rangle]}{\bar{\ell}_f \Sigma_{t_{(f)}}(E)} [1 + \langle G_m \rangle \langle G_f \rangle + (\langle G_m \rangle \langle G_f \rangle)^2 + \ldots]$$

$$= \frac{[1 - \langle G_f \rangle][1 - \langle G_m \rangle]}{\bar{\ell}_f \Sigma_{t_{(f)}}(E)[1 - \langle G_f \rangle \langle G_m \rangle]} \qquad (2.3.7)$$

The problem of calculating $P_f(E)$ is now reduced to finding $\langle G_f \rangle$ and $\langle G_m \rangle$. In order to evaluate $\langle G_f \rangle$ a method very similar to one derived by Chao and Martinez [19] is followed.

$$\langle G_f \rangle = \int \exp(-\Sigma_{t_{(f)}} \ell_f) f(\ell_f) d\ell_f$$

where $f(\ell_f)$ is the chord distribution function in the fuel rod. The exponential factor in the integral is expanded in a power series about $\bar{\ell}_f$, defined as the average value of ℓ_f over the distribution of cord lengths, and the terms independent of ℓ_f are removed from under the integral sign to obtain Eq. (2.3.8).

$$\langle G_f \rangle = \exp(-\Sigma_{t_{(f)}} \bar{\ell}_f)[1 + (\Sigma_{t_f} \bar{\ell}_f)^2 \left\langle \left(\frac{\ell_f}{\bar{\ell}_f} - 1\right)^2 \right\rangle - \frac{(\Sigma_{t_{(f)}} \bar{\ell}_f)^3}{3!} \left\langle \left(\frac{\ell_f}{\bar{\ell}_f} - 1\right)^3 \right\rangle + \ldots] \qquad (2.3.8)$$

In Chao and Martinez's method this series is truncated after the second term, and an analytical approximation for A is made. However, since $\langle G_f \rangle$ can be calculated exactly[24], Eq. (2.3.8) can be used simply to obtain a resonable mathematical expression, which can fit to the exact results.

$$\langle G_f \rangle = \exp(-\tau_f)[1 + A\tau_f^2 - B\tau_f^3] \qquad (2.3.9)$$

where τ_f equals $\Sigma_{t_f} \bar{\ell}_f$ and A and B are arbitrary constants chosen to match the exact results. In this work A was chosen equal to 0.1 and B was chosen to equal zero.

$\langle G_m \rangle$ is known as the Dancoff factor. It may be determined by an analytic expression due to Sauer[20] or chosen to match exact Monte Carlo values for $P_f(E)$ using a procedure described by Gelbard.[21]

BGIM makes use of Eq. (2.3.7) to determine $P_f(E)$ with $\langle G_f \rangle$ determined by Eq. (2.3.9) and $\langle G_m \rangle$ as an input function. An extensive comparison of the results of the calculation of $P_f(E)$

using Eq. (2.3.7) with exact Monte Carlo results is given in section (3.7).

2.4. Derivation of Analytical Flux Shape

An analytical expression for the shape of the neutron flux as a function of energy within a multigroup n is derived in this section. This shape (Note, since the flux appears in both the numerator and denominator of the evaluated expressions, only the shape and not the absolute value is required) is used in BGIM to calculate $\Sigma^i_{t_n}$, $K^j_{i_n}$ and the microscopic total, fission and scattering multigroup cross sections.

Recall Eq. (2.2.15)

$$\Sigma_{t_{(m)}}(u)\bar{\phi}^m(u) = (1 - P_m(u))S_m(u) + \frac{V_f}{V_m} P_f(u)\, S_f(u)$$

$$\Sigma_{t_{(f)}}(u)\bar{\phi}^f(u) = (1 - P_f(u))S_f(u) + \frac{V_m}{V_f} P_m(u)S_m(u) \qquad (2.4.1)$$

where we have used the following definition

$$S_i \equiv \sum_j S_i^j \qquad (2.4.2)$$

Eq. (2.4.1) is chosen as the starting point for the derivation of an expression for $\bar{\phi}^f(u)$. A similar treatment may be used to obtain $\bar{\phi}^m(u)$. Using the reciprocity relationship (2.3.4), Eq. (2.4.3) is obtained for $P_m(u)$.

$$P_m(u) = \frac{V_f}{V_m} \frac{\Sigma_{t_{(f)}}(u)}{\Sigma_{t_{(m)}}(u)} P_f(u) \qquad (2.4.3)$$

Substituting Eq. (2.4.3) into Eq. (2.4.1), dividing through by $\Sigma_{t_{(f)}}(u)$, and cancelling terms, Eq. (2.4.4) is obtained for $\bar{\phi}^f(u)$.

$$\bar{\phi}^f(u) = \frac{(1 - P_f(u))}{\Sigma_{t_{(f)}}(u)} S_f(u) + \frac{P_f(u)}{\Sigma_{t_{(m)}}(u)} S_m(u) \qquad (2.4.4)$$

In order to derive an expression for $\bar{\phi}^f(u)$ assumptions must be made to obtain $S_f(u)$ and $S_m(u)$. Following the reasoning that most of the neutrons appearing in the lethargy range du as a result of scattering from lower lethargies come from lethargy ranges where the absorption cross section is small, the scattering cross section is constant and the total mean free path is large compared to the cell dimension; therefore assumption (2.4.5) is made.

$$S_m(u) = C_n \Sigma^p_{S_{(m)}}$$

$$S_f(u) = C_n \Sigma^p_{S_{(f)}} \qquad (2.4.5)$$

where C_n is a constant for a given multigroup and $\Sigma^p_{S_{(m)}}$ and $\Sigma^p_{S_{(f)}}$ are the macroscopic potential scattering cross sections of the moderator and fuel respectively.

Inserting Eqs.(2.4.5) into Eq. (2.4.4), Eq. (2.4.6) is obtained.

$$\bar{\phi}^f(u) = C_n \frac{(1 - P_f(u))}{\Sigma_{t_f}(u)} \Sigma^p_{S_{(f)}} + \frac{C_n P_f(u)}{\Sigma_{t_m}(u)} \Sigma^p_{S_{(m)}} \qquad (2.4.6)$$

Finally defining

$$C^*_n = C_n \Sigma^p_{S_{(f)}}, \qquad (2.4.7)$$

the following equation for the flux in the fuel as a function of lethargy is obtained. The value of C^*_n cancels in our expressions and need not be known.

$$\bar{\phi}^f(u) = C^*_n \left(\frac{(1 - P_f(u))}{\Sigma_{t_{(f)}}(u)} + \frac{P_f(u)}{\Sigma^p_{S_{(f)}}} \frac{\Sigma^p_{S_{(m)}}}{\Sigma_{t_m}(u)} \right) \qquad (2.4.8)$$

It is of interest to note that near a resonance peak as $P_f(u)$ approaches zero Eq. (2.4.8) reduces to

$$\bar{\phi}^f(u) = \frac{C^*_n}{\Sigma_{t_{(f)}}(u)} \qquad (2.4.9)$$

which is an asymptotic expression that has been used (29) to obtain weighted cross sections.

2.5. Recurrence Relationships and Source Initialization

The solution of Eq. (2.2.30) requires the determination of initial values for $SUM^j_{i_n}$ and $S^H_{m_n}$ and the development of efficient recurrence relationships for calculating $SUM^j_{i_{n+1}}$ and $S^H_{m_{n+1}}$. A set of recurrence relationships is derived in this section which allows computer running time to be proportional to the number of lethargy groups. The brute force method for the calculation of sources without any recurrence relationships is nearly proportional to the square of the total number of groups. A simple method for determining initial values of the sources from a MUFT type solution is also explained in this section.

The hydrogen source in the moderator for an arbitrary n^{th} group is given in general by Eq. (2.5.1)

$$\overline{S^H_{m_n}} = \sum_{k=1}^{n-1} P_k \Sigma^H S_{n-k} \bar{\phi}^m_{n-k} \Delta u \qquad (2.5.1)$$

where

$P_k \equiv$ probability per unit lethargy that a neutron is scattered down k groups in a scattering collision with hydrogen.

$$\overline{S^H_{m_n}} = S^H_{m_n} \Delta u$$

Now since $P_k = e^{-\Delta u} P_{k-1}$, Eq. (2.5.1) can be reduced to

$$\overline{S^H_{m_n}} = e^{-\Delta u} \overline{S^H_{m_{n-1}}} + P_1 \Sigma^H S_{n-1} \bar{\phi}^m_{n-1} \Delta u - e^{-\Delta u} P_n \Sigma^H S_o \bar{\phi}^m_o \Delta u \qquad (2.5.2)$$

Now for hydrogen P_n will be very small so all that is needed is an expression for P_1 . Recalling Eq. (2.2.9) the probability of a neutron being scattered through one group of width Δu is then

$$P_1^{\Delta u} = \int_{u_o}^{u_o+\Delta u} du \int_{u_o-\Delta u}^{u_o} du' \exp(-(u-u'))$$

$$= (1 - e^{-\Delta u})^2 \tag{2.5.3}$$

$$\approx (1 - e^{-\Delta u})\Delta u$$

Finally, a recurrence relationship for the hydrogen source can be written.

$$\overline{S^H_{m_{n+1}}} = e^{-\Delta u}\, \overline{S^H_{m_n}} + \Delta u(1 - e^{-\Delta u})\Sigma^H_{S_n} \phi^m_n \tag{2.5.4}$$

The definition of $SUM^j_{i_n}$ is recalled in Eq. (2.5.5).

$$SUM^j_{i_n} \equiv \sum_{\ell=1}^{L^j} K^j_{i_{n-\ell}}\, \bar{\phi}^i_{n-\ell}\, \Delta u \tag{2.5.5}$$

The recurrence relationship for this quantity follows directly from this definition and is given in Eq. (2.5.6).

$$SUM^{j}_{i_{n+1}} = SUM^{j}_{i_n} - K^{j}_{i_{n-L_j}} \bar{\phi}^{i}_{n-L_j\Delta} + K^{j}_{i_n} \bar{\phi}^{i}_{n\Delta} \qquad (2.5.6)$$

Initial values of S^{H}_{mI} and SUM^{j}_{iI} can be chosen based on input from a MUFT-type code. The BGIM solution is not sensitive to the absolute values of these quantities, so a reasonable approximation will be adequate. This is accomplished by considering three types of isotopes, heavy (e.g. U238), intermediate (e.g. 016) and hydrogen.

For hydrogen

$$S^{H}_{nI} = \int_{o}^{u_I} e^{-(u-u')} \Sigma^{H}_{S_m}(u') \bar{\phi}^{m}(u') du' \qquad (2.5.7)$$

S^{H}_{nI} is an input quantity in BGIM and can be derived by breaking up the integral in Eq. (2.5.7) into a sum of integrals over the MUFT type code microgroups and assuming $\bar{\phi}^{m}(u')$ is constant within a microgroup.

The initial values of $SUM^{j}_{i_n}$ can be calculated directly from definition (2.5.5). The fluxes at lethargies lower than the initial value of u_I can be calculated using Eq. (2.5.8) for the heavy isotopes and using the MUFT-type code values of flux for the intermediate isotopes assuming the flux to be constant within a microgroup.

$$\bar{\phi}^{i}_{I} = \frac{q(u_I)}{\xi \Sigma_s} \qquad (2.5.8)$$

where

$q(u_I)$ ≡ the slowing down density at u_I

2.6. Description of BGIM Code

A computer code called BGIM has been developed to test the theory outlined in sections 2.1 to 2.5. BGIM was written only as a means of testing the theory we have given and is not intended for use as a production code. However, in order that references to the results of the BGIM code given in the next chapter can be understood more clearly, a list of the subroutines in BGIM and what they do will be given. Also, a short discussion of the options and output of the BGIM code will be made.

The subroutines in the BGIM code are as follows:

RINPUT - This subroutine reads the card input which contains data such as number densities and option designators. It also reads a tape file of VIM microscopic pointwise cross sections.

WORK - This subroutine uses a Simpson's rule integration to obtain the integral multigroup parameters such as $K^j_{f_n}$ etc., which are needed as input to solve Eq. (2.2.30). Linear interpolation of the VIM pointwise cross section file is used to obtain a continuous cross section description in energy. Thus, the choice of integration step size and multigroup lethargy width are arbitrary.

SOURCE - This subroutine calculates the initial hydrogen source and the starting values for $SUM^j_{i_n}$.

RITE - This subroutine writes out the multigroup parameters calculated by WORK to a disk file.

DINPUT - This subroutine reads a disk file created by RITE.

SOLVE - This subroutine uses a stepping-up-in-lethargy procedure to solve Eq. (2.2.30). It also uses the recurrence relationships given in section 2.5 to calculate $SUM^j_{i_{n+1}}$ and $S^H_{i_{n+1}}$.

EDIT - This subroutine performs the output editing.

INTERP - This subroutine performs a linear interpolation.

PPF - This is a function subroutine that calculates escape probabilities. It uses Eq. (2.3.7) with $\langle G_f \rangle$ given by Eq. (2.3.9) and $\langle G_m \rangle$ as an input function.

FL - This is a function subroutine that calculates the flux shape using Eq. (2.4.8). Simpler or more exact equations for the flux shape can easily be used in BGIM by reprogramming this function subroutine.

The major BGIM options are:

1. Choice of Simpson's Rule integration step size.
2. Choice of multigroup lethargy width.

3. Choice of energy range of solution, which must be below 300 ev. and above 1.855 ev.

4. Choice of performing a heterogeneous or a homogeneous cell calculation.

5. Choice of the calculation of the multigroup parameters. They may be calculated directly from the VIM cross section file using WORK, or they may be read by DINPUT from a previously WORK-RITE created disk file.

The BGIM output consists of:

1. The macroscopic groups constants $\nu\Sigma_f$, Σ_a, Σ_r and the microscopic cross section σ_f and σ_a averaged over the energy range of solution.

2. The flux, and absorption and fission rates by isotope integrated over the energy range of solution.

3. BGIM also calculates the above data over an arbitrary user input set of lethargy groups. Up to 200 groups may be specified.

3. RESULTS

3.1. Problem Types

This section defines the isotopic concentrations, lattice geometry and temperatures that are used in this study. The isotopic concentrations in the pellet are designated as fuel types. The lattice geometry, moderator temperature, and moderator isotopics are designated as lattice types.

Table 5. Fuel Type 1

Fuel Temperature 300°K

Isotope	Pellet Number Density (1/barn-cm)
016	45192-1
U238	20735-1
Pu239	10905-2

Description: These isotopes represent concentrations that would be found at BOL (Beginning of Life) in a 8 w/o enriched PuO_2-UO_2 pellet. In this Table and those following numbers such as 0.45192×10^{-1} will be represented as 45192-1.

Table 6. Fuel Type 2

Fuel Temperature 300°K

Isotope	Pellet Number Density (1/barn-cm)
016	43346-1
U238	203030-1
Pu239	13700-2

Description: These isotopes represent concentrations that would be found at BOL in a 10 w/o enriched PuO_2-UO_2 pellet.

Table 7. Fuel Type 3

Fuel Temperature 300°K

Isotope	Pellet Number Density (1/barn-cm)
016	45264-1
U238	19870-1
Pu239	16454-2

Description: These isotopes represent concentrations that would be found at BOL in a 12 w/o enriched PuO_2-UO_2 pellet.

Table 3. Fuel Type 4

Fuel Temperature 1000°K

Isotope	Pellet Number Density (1/barn-cm)
016	43346-1
U238	20303-1
Pu239	13700-2
Pu240	20303-3

Description: These isotopes represent concentrations that would be found at BOL in a 10 w/o enriched PuO_2-UO_2 pellet.

Table 9. Fuel Type 5

Fuel Temperature 1000°K

Isotope	Pellet Number Density (1/barn-cm)
016	43346-1
U238	20238-1
Pu239	13586-2
Pu240	46642-3

Description: These isotopes represent concentrations that would be found at 2,500 MWD/MTM in a 10 w/o enriched PuO_2-UO_2 pellet.

Table 10. Fuel Type 6

Fuel Temperature 1000°K

Isotope	Pellet Number Density (1/barn-cm)
016	43346-1
U238	20067-1
Pu239	13381-2
Pu240	48890-3

Description: These isotopes represent concentrations that would be found at 10,000 MWD/MTM in a 10 w/o enriched PuO_2-UO_2 pellet.

Table 11. Fuel Type 7

Fuel Temperature 1000°K

Isotope	Pellet Number Density (1/barn-cm)
016	43340-1
U238	19833-1
Pu239	13145-2
Pu240	51753-3

Description: These isotopes represent concentrations that would be found at 20,000 MWD/MTM in a 10 w/o enriched PuO_2-UO_2 pellet.

Table 12. Fuel Type 8

Fuel Temperature 1000°K

Isotope	Pellet Number Density (1/barn-cm)
O16	43346-1
U238	19098-1
Pu239	12621-2
Pu240	59338-3

Description: These isotopes represent concentrations that would be found at 50,000 MWD/MTM in a 10 w/o enriched PuO_2-UO_2 pellet.

Table 13. Lattice Type 1

Cell Type Hexagonal
Pellet Diameter .7162 cm.
Cell Pitch .9144 cm.
Moderator Temperature 73°F

Isotope	Moderator Number Density (1/barn-cm)
H1	41025-1
016	20513-1

Description: This lattice type represents a lattice with a fuel to moderator ratio of 2 to 1. The cladding and moderator are considered to be homogenized and the cladding isotopes are not input.

Table 14. Lattice Type 2

Cell Type Hexagonal
Pellet Diameter .7162 cm.
Cell Pitch .8865 cm.
Moderator Temperature 73°F

Isotope	Moderator Number Density (1/barn-cm)
H1	37343-1
016	18671-1

Description: This lattice type represents a lattice with a fuel to moderator ratio of 2.5 to 1. The cladding and moderator are considered to be homogenized and the cladding isotopes are not input.

Table 15. Lattice Type 3

Cell Type Hexagonal
Pellet Diameter .7162 cm.
Cell Pitch .9783 cm.
Moderator Temperature 73°F

Isotope	Moderator Number Density (1/barn-cm)
H1	46733-1
016	23367-1

Description: This lattice type represents a lattice with a fuel to moderator ratio of 1.3 to 1. The cladding and moderator are considered to be homogenized and the cladding isotopes are not input.

Table 16. Lattice Type 4

Cell Type Hexagonal
Pellet Diameter .7162 cm.
Cell Pitch 1.1809 cm.
Moderator Temperature 73°F

Isotope	Moderator Number Density (1/barn-cm)
H1	.54953-1
016	27477-1

Description: This lattice type represents a lattice with a fuel to moderator ratio of .585 to 1. The cladding and moderator are considered to be homogenized and the cladding isotopes are not input.

Table 17. Lattice Type 5

Cell Type Hexagonal
Pellet Diameter .8382 cm.
Cell Pitch 1.0571 cm.
Moderator Temperature 73°F

Isotope	Moderator Number Density (1/barn-cm)
H1	43456-1
016	21728-1

Description: This lattice type represents a lattice with a fuel to moderator ratio of 2 to 1. The cladding and moderator are considered to be homogenized and the cladding isotopes are not input.

Table 18. Lattice Type 6

Cell Type Hexagonal
Pellet Diameter .7162 cm.
Cell Pitch .9144 cm.
Moderator Temperature 580°F

Isotope	Moderator Number Density (1/barn-cm)
H1	29435-1
016	14717-1

Description: This lattice type represents a lattice with a fuel to moderator ratio of 2 to 1. The cladding and moderator are considered to be homogenized and the cladding isotopes are not input.

3.2. Statistical Accuracy of VIM Results

This section provides an estimate of the statistical accuracy of VIM calculated quantities. Two-sigma values for the principal calculated quantities are given in Table 19. These values are typical of the results obtained in the calculations reported in section 3.5. A typical Monte Carlo run consists of approximately 40 batches of 500 neutron histories. The neutron makes approximately 600,000 collisions during these traces.

The cross sections given in Table 19 are cell and energy averaged. The energy range for these group cross sections is 167 ev to 1.855 ev.

3.3. Analysis of Broad Group Lethargy Widths and Integration Stepsize

BGIM allows a choice of both group lethargy width and integration stepsize. A study is made in this section comparing VIM and BGIM for a variety of group widths and integration step sizes. These results are used to choose a reasonable combination of these parameters to be used in BGIM.

Fuel type 2 and lattice type 1 in a heterogeneous cell are chosen as the base case for this study. VIM is used to calculate this case and is compared with BGIM using a variety of group widths and step sizes. The results of these calculations are given in Table 20.

TABLE 19. Statistical Accuracy of VIM Results

Calculated Quantity	Statistical Variation*
$\nu\Sigma_f$	± 2.6%
Σ_a	± 2.0%
Σ_R	± 3.2%
σ_a^{238}	± 3.0%
σ_a^{239}	± 2.5%
σ_f^{239}	± 2.7%
σ_a^{240}	± 5.0%
σ_f^{240}	± 4.0%
k_∞	± .8%

* The statistical variations are two standard deviation values.

TABLE 20

Effects of Group Width and Integration Stepsize Variation

Integration Stepsize in Lethargy	Group Width in Lethargy	Relative Computer Time	% Diff Σ_a*	% Diff ρ**
.00005	.002	2.9	.34	-.17
.0001	.002	1.50	-.50	-.02
.00025	.002	.70	-3.7	.57
.0005	.002	.40	-14.8	2.58
.00025	.003	.60	-.56	-1.35
.00015	.003	1.0	-.60	-.02
.0005	.003	.37	-6.4	1.04
.0001	.004	1.48	1.74	-.41
.0005	.004	.36	-2.0	2.47
.0001	.005	1.44	1.48	-.43
.0005	.005	.34	-1.17	.02
.0001	.01	1.41	3.08	-.59
.0005	.01	.32	2.15	-.47

* $$\frac{\Sigma_a^{BGIM} - \Sigma_a^{VIM}}{\Sigma_a^{VIM}} \times 100$$

** $$\frac{K^{BGIM} - K^{VIM}}{K^{BGIM}\ K^{VIM}} \times 100$$

The agreement between VIM and BGIM improves as the integration step and group widths are decreased, as expected. The group widths studied are wide compared to the integration size since the whole purpose of this development is to use broad groups. A group width of 0.003 and an integration stepsize 0.00015 are chosen as base values for the remainder of the BGIM calculations.

This choice is made so that the results reported in the remaining sections will be typical of what a nuclear fuel cycle designer might expect when using BGIM on a production basis. Better agreement between VIM and BGIM would be obtained if smaller integration step sizes and group widths were used, but it is felt that the base values give a good balance between accuracy and computing resources.

3.4. Accuracy Gains Achieved Through Use of New Analytic Flux Shape

This section examines the accuracy that is gained through the use of the analytic flux shape derived in section 2.4. Recall Eq. (2.4.8) for the analytic flux shape used by BGIM

$$\bar{\phi}^{f}(u) = C_n^* \left[\frac{(1 - P_f(u))}{\Sigma_{t(f)}(u)} + \frac{P_f(u)}{\bar{\Sigma}^{P}_{S(f)}} \frac{\Sigma^{P}_{S(m)}}{\Sigma_{t(m)}} \right] \qquad (3.4.1)$$

Near resonance peaks, as $P_f(u)$ approaches zero, Eq. (3.4.1) reduces to the asymptotic form (3.4.2). This flux shape has been used in the past to obtain weighted cross sections.

$$\phi^{f}(u) = \frac{C_n^*}{\Sigma_{t(f)}(u)} \qquad (3.4.2)$$

This flux shape was also programmed into BGIM in order to evaluate the validity and worth of Eq. (3.4.1). A heterogeneous cell with fuel type 2 in lattice type 1 was used for this evaluation. The results showed significant gains in accuracy can be achieved through use of Eq. (3.4.1).

The VIM results were considered as reference values and the BGIM calculations using both Eq. (3.4.1) and Eq. (3.4.2) were compared with VIM results. The macroscopic absorption cross section in the range 1.855 ev to 167 ev was overestimated by 3.27% using Eq. (3.4.2) but underestimated by only .6% using Eq. (3.4.1). The overall system reactivity was overestimated by 1.16% $\Delta\rho$ using Eq. (3.4.2) and underestimated by only .02% $\Delta\rho$ using Eq. (3.4.1).

The most significant fact about improvements made through the use of Eq. (3.4.1) is that these gains come with very little complexity added to the calculation. This is true since all the quantities in Eq. (3.4.1) are already needed by BGIM. Hence, they are pre-computed and stored in memory when the evaluation of Eq. (3.4.1) is made.

3.5. Verification of the BGIM Theory

This section gives the results of a comprehensive test of the BGIM Theory. Extensive comparisons are made between the VIM and BGIM codes in order to show the validity of the BGIM assumptions. These results presented in tabular form show excellent agreement in all cases and thereby verify the adequacy of the BGIM Theory.

Heterogeneous and homogeneous cell calculations are performed for a variety of enrichments, burnups, lattice spacings, temperatures and isotopic variations. Tables 21 through 26 give the results for enrichment variations. Tables 27 through 30 give the results for single isotope calculations. Tables 31 through 34 give the results for lattice variations. Table 35 shows the effect of temperature and burnup variation.

The isotopics used for this study were limited to H1, O16, U238, Pu239 and Pu240. This was done in order to simplify the programming of the BGIM code. These isotopes show all of the complex resonance overlaps and interferences that can occur in the lower resolved resonance range, so very little information is lost by limiting the analysis to these isotopes.

The data tables are for the most part self-explanatory but a few additional comments are given for further clarification:

1. The cross sections are space averaged over an infinite array of pin cells, and energy averaged over the range 1.855 ev - 167 ev.

TABLE 21 HETERO CELL FUEL TYPE 1 LATTICE 1

MACROSCOPIC GROUP CONSTANTS

	NU SIG-F	SIG-A	SIG-R
VIM	0.54155E-01	0.67176E-01	0.72080E-01
BGIM	0.52622E-01	0.65910E-01	0.73233E-01
% DIF	-0.28308E 01	-0.13346E 01	0.15996E 01

MICROSCOPIC GROUP CONSTANTS

ISOTOPE 238

	SIG-F	SIG-A
VIM	0.22353E-07	0.30867E 01
BGIM	0.21739E-07	0.30504E 01
% DIF	-0.27468E 01	-0.11760E 01

ISOTOPE 239

	SIG-F	SIG-A
VIM	0.30930E 02	0.51369E 02
BGIM	0.30169E 02	0.50560E 02
% DIF	-0.24604E 01	-0.15749E 01

REACTIVITY ANALYSIS

	KIN-F
VIM	0.12536E 01
BGIM	0.12571E 01
% DELTA RHO	0.21756E 00

TABLE 22 HOMO CELL FUEL TYPE 1 LATTICE TYPE 1

MACROSCOPIC GROUP CONSTANTS

	NU SIG-F	SIG-A	SIG-R
VIM	0.57121E-01	0.73413E-01	0.69381E-01
BGIM	0.56093E-01	0.72993E-01	0.69314E-01
% DIF	-0.17997E 01	-0.57215E 00	-0.96562E-01

MICROSCOPIC GROUP CONSTANTS

ISOTOPE 238

	SIG-F	SIG-A
VIM	0.22253E-07	0.34427E 01
BGIM	0.22202E-07	0.34714E 01
% DIF	-0.22739E 00	0.83364E 00

ISOTOPE 239

	SIG-F	SIG-A
VIM	0.32625E 02	0.54884E 02
BGIM	0.32044E 02	0.54065E 02
% DIF	-0.17808E 01	-0.14922E 01

REACTIVITY ANALYSIS

	KIN-F
VIM	0.12128E 01
BGIM	0.12102E 01
% DELTA RHO	-0.17746E 00

TABLE 23 HETERO CELL FUEL TYPE 2 LATTICE TYPE 1

MACROSCOPIC GROUP CONSTANTS

	NU SIG-F	SIG-A	SIG-R
VIM	0.63720E-01	0.71464E-01	0.71900E-01
BGIM	0.62699E-01	0.71033E-01	0.72712E-01
% DIF	-0.16023E 01	-0.60310E 00	0.11293E 01

MICROSCOPIC GROUP CONSTANTS

ISOTOPE 238

	SIG-F	SIG-A
VIM	0.22141E-07	0.30349E 01
BGIM	0.21552E-07	0.30736E 01
% DIF	-0.26602E 01	0.12752E 01

ISOTOPE 239

	SIG-F	SIG-A
VIM	0.29088E 02	0.48429E 02
BGIM	0.28612E 02	0.47580E 02
% DIF	-0.16364E 01	-0.17531E 01

REACTIVITY ANALYSIS

	KIN-F
VIM	0.13019E 01
BGIM	0.13016E 01
% DELTA RHO	-0.19417E-01

TABLE 24 HOMO CELL FUEL TYPE 2 LATTICE TYPE 1

MACROSCOPIC GROUP CONSTANTS

	NU SIG-F	SIG-A	SIG-R
VIM	0.68621E-01	0.79899E-01	0.69786E-01
BGIM	0.67221E-01	0.79016E-01	0.68889E-01
% DIF	-0.20402E 01	-0.11052E 01	-0.12853E 01

MICROSCOPIC GROUP CONSTANTS

ISOTOPE 238

	SIG-F	SIG-A
VIM	0.22099E-07	0.35259E 01
BGIM	0.21864E-07	0.35227E 01
% DIF	-0.10634E 01	-0.90745E-01

ISOTOPE 239

	SIG-F	SIG-A
VIM	0.31326E 02	0.52232E 02
BGIM	0.30693E 02	0.51451E 02
% DIF	-0.20207E 01	-0.14952E 01

REACTIVITY ANALYSIS

	KIN-F
VIM	0.12897E 01
BGIM	0.12864E 01
% DELTA RHO	-0.19862E 00

TABLE 25 HETERO CELL FUEL TYPE 3 LATTICE TYPE 1

MACROSCOPIC GROUP CONSTANTS

	NU SIG-F	SIG-A	SIG-R
VIM	0.73970E-01	0.76567E-01	0.72180E-01
BGIM	0.72231E-01	0.76090E-01	0.72240E-01
% DIF	-0.23510E 01	-0.62300E 00	0.83156E-01

MICROSCOPIC GROUP CONSTANTS

ISOTOPE 238

	SIG-F	SIG-A
VIM	0.21929E-07	0.30463E 01
BGIM	0.21379E-07	0.31221E 01
% DIF	-0.25081E 01	0.24883E 01

ISOTOPE 239

	SIG-F	SIG-A
VIM	0.28116E 02	0.46558E 02
BGIM	0.27445E 02	0.45360E 02
% DIF	-0.23865E 01	-0.25731E 01

REACTIVITY ANALYSIS

	KIN-F
VIM	0.13350E 01
BGIM	0.13306E 01
% DELTA RHO	-0.26743E 00

TABLE 26 HOMO CELL FUEL TYPE 3 LATTICE TYPE 1

MACROSCOPIC GROUP CONSTANTS

	NU SIG-F	SIG-A	SIG-R
VIM	0.77416E-01	0.84372E-01	0.68480E-01
BGIM	0.77494E-01	0.84315E-01	0.67766E-01
% DIF	0.10078E 00	-0.67537E-01	-0.10426E 01

MICROSCOPIC GROUP CONSTANTS

ISOTOPE 238

	SIG-F	SIG-A
VIM	0.21954E-07	0.35524E 01
BGIM	0.21736E-07	0.35619E 01
% DIF	-0.99299E 00	0.26744E 00

ISOTOPE 239

	SIG-F	SIG-A
VIM	0.29425E 02	0.48984E 02
BGIM	0.29461E 02	0.49080E 02
% DIF	0.12233E 00	0.19600E 00

REACTIVITY ANALYSIS

	KIN-F
VIM	0.12913E 01
BGIM	0.12904E 01
% DELTA RHO	-0.52194E-01

TABLE 27 HETERO CELL FUEL TYPE 2 U238 LATTICE TYPE 1

MACROSCOPIC GROUP CONSTANTS

	NU SIG-F	SIG-A	SIG-R
VIM	0.10000E-09	0.34461E-01	0.78780E-01
BGIM	0.10000E-09	0.34166E-01	0.77353E-01
% DIF	0.00000E 00	-0.85604E 00	-0.18114E 01

MICROSCOPIC GROUP CONSTANTS

ISOTOPE 238

	SIG-F	SIG-A
VIM	0.23396E-07	0.30265E 01
BGIM	0.23002E-07	0.30227E 01
% DIF	-0.16841E 01	-0.12554E 00

REACTIVITY ANALYSIS

	KIN-F
VIM	0.14925E 00
BGIM	0.14925E 00
% DELTA RHO	0.26759E-03

TABLE 28 HOMO CELL FUEL TYPE 2 U236 LATTICE TYPE 1

MACROSCOPIC GROUP CONSTANTS

	NU SIG-F	SIG-A	SIG-R
VIM	0.10000E-09	0.39038E-01	0.75230E-01
BGIM	0.10000E-09	0.38923E-01	0.75009E-01
% DIF	0.00000E 00	-0.29453E 00	-0.29378E 00

MICROSCOPIC GROUP CONSTANTS

	ISOTOPE 238	
	SIG-F	SIG-A
VIM	0.23287E-07	0.34325E 01
BGIM	0.23082E-07	0.34455E 01
% DIF	-0.88033E 00	0.37875E 00

REACTIVITY ANALYSIS

	KIN-F
VIM	0.14932E 00
BGIM	0.14932E 00
% DELTA RHO	0.00000E 00

TABLE 29 HETERO CELL FUEL TYPE 2 PU239 LATTICE TYPE 1

MACROSCOPIC GROUP CONSTANTS

	NU SIG-F	SIG-A	SIG-R
VIM	0.57263E-01	0.32538E-01	0.78530E-01
BGIM	0.58785E-01	0.33546E-01	0.78456E-01
% DIF	0.26579E 01	0.30979E 01	-0.94268E-01

MICROSCOPIC GROUP CONSTANTS

ISOTOPE 239

	SIG-F	SIG-A
VIM	0.26141E 02	0.42326E 02
BGIM	0.26826E 02	0.43982E 02
% DIF	0.26204E 01	0.39076E 01

REACTIVITY ANALYSIS

	K1N-F
VIM	0.18790E 01
BGIM	0.18765E 01
% DELTA RHO	-0.69861E-01

TABLE 30 HOMO CELL FUEL TYPE 2 PU239 LATTICE TYPE 1

MACROSCOPIC GROUP CONSTANTS

	NU SIG-F	SIG-A	SIG-R
VIM	0.62914E-01	0.36257E-01	0.78587E-01
BGIM	0.62652E-01	0.36052E-01	0.79251E-01
% DIF	-0.41648E 00	-0.56541E 00	0.84492E 00

MICROSCOPIC GROUP CONSTANTS

ISOTOPE 239

	SIG-F	SIG-A
VIM	0.28721E 02	0.47211E 02
BGIM	0.28607E 02	0.47293E 02
% DIF	-0.39692E 00	0.17369E 00

REACTIVITY ANALYSIS

	KIN-F
VIM	0.18452E 01
BGIM	0.18462E 01
% DELTA RHO	0.28607E-01

TABLE 31 HETERO CELL FUEL TYPE 2 LATTICE TYPE 2

MACROSCOPIC GROUP CONSTANTS

	NU SIG-F	SIG-A	SIG-R
VIM	0.65686E-01	0.73275E-01	0.60348E-01
BGIM	0.65248E-01	0.72943E-01	0.59145E-01
% DIF	-0.66677E 00	-0.45317E 00	-0.19934E 01

MICROSCOPIC GROUP CONSTANTS

ISOTOPE	238	
	SIG-F	SIG-A
VIM	0.21657E-07	0.29183E 01
BGIM	0.21210E-07	0.29300E 01
% DIF	-0.20640E 01	0.40094E 00

ISOTOPE	239	
	SIG-F	SIG-A
VIM	0.28184E 02	0.46834E 02
BGIM	0.27971E 02	0.46415E 02
% DIF	-0.75579E 00	-0.89466E 00

REACTIVITY ANALYSIS

	KIN-F
VIM	0.12616E 01
BGIM	0.12587E 01
% DELTA RHO	-0.18545E 00

TABLE 32 HETERO CELL FUEL TYPE 2 LATTICE TYPE 3

MACROSCOPIC GROUP CONSTANTS

	NU SIG-F	SIG-A	SIG-R
VIM	0.57266E-01	0.66676E-01	0.99108E-01
BGIM	0.56727E-01	0.66560E-01	0.99650E-01
% DIF	-0.94122E 00	-0.47255E 00	0.54692E 00

MICROSCOPIC GROUP CONSTANTS

ISOTOPE 238

	SIG-F	SIG-A
VIM	0.22589E-07	0.33524E 01
BGIM	0.22200E-07	0.34038E 01
% DIF	-0.17216E 01	0.15332E 01

ISOTOPE 239

	SIG-F	SIG-A
VIM	0.29924E 02	0.50208E 02
BGIM	0.29647E 02	0.49497E 02
% DIF	-0.92565E 00	-0.14161E 01

REACTIVITY ANALYSIS

	KIN-F
VIM	0.13683E 01
BGIM	0.13689E 01
% DELTA RHO	0.28360E-01

TABLE 33 HETERO CELL FUEL TYPE 2 LATTICE 4

MACROSCOPIC GROUP CONSTANTS

	NU SIG-F	SIG-A	SIG-R
VIM	0.42419E-01	0.50971E-01	0.16053E 00
BGIM	0.40790E-01	0.50402E-01	0.15957E 00
% DIF	-0.38403E 01	-0.11163E 01	-0.59801E 00

MICROSCOPIC GROUP CONSTANTS

ISOTOPE 238

	SIG-F	SIG-A
VIM	0.23222E-07	0.38327E 01
BGIM	0.22462E-07	0.39185E 01
% DIF	-0.31866E 01	0.22386E 01

ISOTOPE 239

	SIG-F	SIG-A
VIM	0.32297E 02	0.53515E 02
BGIM	0.31048E 02	0.52151E 02
% DIF	-0.38672E 01	-0.25438E 01

REACTIVITY ANALYSIS

	KIN-F
VIM	0.15278E 01
BGIM	0.15238E 01
% DELTA RHO	-0.16845E 00

TABLE 34 HETERO CELL FUEL TYPE 2 LATTICE TYPE 5

MACROSCOPIC GROUP CONSTANTS

	NU SIG-F	SIG-A	SIG-R
VIM	0.64017E-01	0.72210E-01	0.75488E-01
BGIM	0.63732E-01	0.72467E-01	0.75099E-01
% DIF	-0.44515E 00	0.35595E 00	-0.51529E 00

MICROSCOPIC GROUP CONSTANTS

ISOTOPE 238

	SIG-F	SIG-A
VIM	0.22164E-07	0.30182E 01
BGIM	0.21545E-07	0.30761E 01
% DIF	-0.27928E 01	0.19184E 01

ISOTOPE 239

	SIG-F	SIG-A
VIM	0.28521E 02	0.47373E 02
BGIM	0.28394E 02	0.47170E 02
% DIF	-0.44528E 00	-0.42852E 00

REACTIVITY ANALYSIS

	KIN-F
VIM	0.13055E 01
BGIM	0.13018E 01
% DELTA RHO	-0.21970E 00

TABLE 35 HETERO CELL FUEL TYPE 6 LATTICE TYPE 6

MACROSCOPIC GROUP CONSTANTS

	NU SIG-F	SIG-A	SIG-R
VIM	0.64828E-01	0.78375E-01	0.48599E-01
BGIM	0.63488E-01	0.77290E-01	0.49280E-01
% DIF	-0.20670E 01	-0.13843E 01	0.14013E 01

MICROSCOPIC GROUP CONSTANTS

ISOTOPE 238

	SIG-F	SIG-A
VIM	0.21191E-07	0.30851E 01
BGIM	0.20809E-07	0.30964E 01
% DIF	-0.18026E 01	0.37274E 00

ISOTOPE 239

	SIG-F	SIG-A
VIM	0.30251E 02	0.51506E 02
BGIM	0.29624E 02	0.50247E 02
% DIF	-0.20727E 01	-0.24444E 01

ISOTOPE 240

	SIG-F	SIG-A
VIM	0.13289E 00	0.20110E 02
BGIM	0.13102E 00	0.19332E 02
% DIF	-0.14072E 01	-0.38687E 01

REACTIVITY ANALYSIS

	KIN-F
VIM	0.98494E 00
BGIM	0.98370E 00
% DELTA RHO	-0.12638E 00

2. K_∞ is calculated using three group theory for an infinite system with groups one and three obtained from VIM and group two (1.855 ev - 167 ev) obtained from either VIM or BGIM as indicated.

3. The lattice and fuel type designations are explained in Section 3.1.

4. The statistical variations for the VIM calculations are given in Section 3.2.

5. The % Diff is defined as

$$\frac{\text{BGIM} - \text{VIM}}{\text{VIM}} * 100$$

6. % Delta Rho is defined as

$$\frac{K_\infty^{BGIM} - K_\infty^{VIM}}{K_\infty^{BGIM} K_\infty^{VIM}} * 100$$

These results prove the validity of the BGIM Theory. The method works over a broad range of conditions and shows no large errors or biases when compared to the benchmark code, VIM. The major observations made from these results are:

1. No major observable trends exist in the differences between the results of BGIM and VIM.

2. Almost all results from BGIM are within the statistical errors of the VIM calculations.

3. Homogeneous and heterogeneous cells were calculated with equal accuracy which indicates that the spatial shielding calculation made using escape probabilities is not adding appreciable errors to the results.

4. Single and multiple isotope calculations show no major discernable error trends. This indicates that resonance overlap and interference are being treated well.

5. There is a small but detectable trend of reactivity difference vs. plutonium enrichment (See Tables 21, 23, 25). This reflects the increased shielding of the Pu resonances and the increased contribution of the Pu isotopes to the total absorption.

3.6. MBGIM (mini-BGIM) Method

This section describes a simplification of the BGIM Method which is designated MBGIM (mini-BGIM). MBGIM is an option of the BGIM program (See Section 2.6) which uses previously calculated values for the microscopic integral multigroup parameters (Eq. K^{j}_{fn} etc.). These microscopic integral multigroup parameters are assumed to be constant for small changes in isotopics. Therefore, they can be calculated for a base case, stored on a disk file, and used for various calculations with similar isotopics. The MBGIM option reads these parameters from disk and multiplies them by the isotopic number densities to obtain the integral macroscopic multigroup parameters required by Eq. (2.2.30). It should be noted that the escape probability integrals are not microscopic quantities. MBGIM assumes

that they are unchanged from the base case when solving Eq. (2.2.30).

MBGIM is tested primarily as an option that would be used for a fuel cycle unit cell depletion calculation with the full BGIM treatment being used to generate the multigroup parameters every few burnup steps. The results of these tests not only confirm the adequacy of MBGIM for a fuel cycle unit cell depletion calculation, but also indicate that MBGIM might be used over a broader range.

The first set of test cases consists of running a full BGIM calculation at 0 MWD/MTM to generate multigroup parameters for MBGIM. MBGIM using the 0 MWD/MTM parameters is compared to the full BGIM treatment for 2500, 10,000, 20,000 and 50,000 MWD/MTM in Tables 36 - 39. These results show that very few full BGIM calculations are needed during a fuel cycle unit cell depletion calculation. In fact, a single BOL, BGIM calculation seems sufficient.

The second set of test cases consists of running a full BGIM calculation for 10 w/o Pu to generate multigroup parameters for MBGIM. MBGIM using the 10 w/o Pu parameters is compared to the full BGIM treatment for 8 w/o and 12 w/o Pu in Table 40 and 41. These results show that the errors obtained, when the isotopes are changed through enrichment variations, are greater than those for the fuel cycle unit cell depletion calculation. However, these errors might be tolerable (a maximum error in σ_a^{239} of 3%). This suggests that a generic set of integral microscopic multigroup parameters could be calculated using BGIM that could be used by MBGIM over a broad range of fuel compositions. This would result in a great savings in

TABLE 36 HETERO CELL FUEL TYPE 5 LATTICE TYPE 6

MACROSCOPIC GROUP CONSTANTS

	NU SIG-F	SIG-A	SIG-R
VIM	0.64241E-01	0.77724E-01	0.49232E-01
BGIM	0.64331E-01	0.77780E-01	0.49160E-01
% DIF	0.14010E 00	0.72086E-01	-0.14624E 00

MICROSCOPIC GROUP CONSTANTS

ISOTOPE 238

	SIG-F	SIG-A
VIM	0.20792E-07	0.30852E 01
BGIM	0.20806E-07	0.30859E 01
% DIF	0.67322E-01	0.22689E-01

ISOTOPE 239

	SIG-F	SIG-A
VIM	0.29525E 02	0.50075E 02
BGIM	0.29567E 02	0.50145E 02
% DIF	0.14228E 00	0.13980E 00

ISOTOPE 240

	SIG-F	SIG-A
VIM	0.13249E 00	0.19588E 02
BGIM	0.13243E 00	0.19571E 02
% DIF	-0.45258E-01	-0.86779E-01

REACTIVITY ANALYSIS

	KIN-F
VIM	0.98538E 00
BGIM	0.98552E 00
% DELTA RHO	0.14448E-01

TABLE 37 HETERO CELL FUEL TYPE 6 LATTICE TYPE 6

MACROSCOPIC GROUP CONSTANTS

	NU SIG-F	SIG-A	SIG-R
VIM	0.63468E-01	0.77296E-01	0.49280E-01
BGIM	0.63750E-01	0.77448E-01	0.49055E-01
% DIF	0.41271E 00	0.20444E 00	-0.45657E 00

MICROSCOPIC GROUP CONSTANTS

ISOTOPE 238

	SIG-F	SIG-A
VIM	0.20809E-07	0.30966E 01
BGIM	0.20856E-07	0.30989E 01
% DIF	0.22586E 00	0.74283E-01

ISOTOPE 239

	SIG-F	SIG-A
VIM	0.29624E 02	0.50247E 02
BGIM	0.29747E 02	0.50452E 02
% DIF	0.41521E 00	0.40799E 00

ISOTOPE 240

	SIG-F	SIG-A
VIM	0.13102E 00	0.19332E 02
BGIM	0.13072E 00	0.19256E 02
% DIF	-0.22897E 00	-0.38383E 00

REACTIVITY ANALYSIS

	KIN-F
VIM	0.98370E 00
BGIM	0.98412E 00
% DELTA RHO	0.43346E-01

TABLE 38 HETERO CELL FUEL TYPE 7 LATTICE TYPE 6

MACROSCOPIC GROUP CONSTANTS

	NU SIG-F	SIG-A	SIG-R
VIM	0.62614E-01	0.76767E-01	0.49339E-01
BGIM	0.63082E-01	0.77050E-01	0.48913E-01
% DIF	0.74737E 00	0.36857E 00	-0.86342E 00

MICROSCOPIC GROUP CONSTANTS

ISOTOPE 238

	SIG-F	SIG-A
VIM	0.20829E-07	0.31128E 01
BGIM	0.20920E-07	0.31174E 01
% DIF	0.43690E 00	0.14779E 00

ISOTOPE 239

	SIG-F	SIG-A
VIM	0.29739E 02	0.50444E 02
BGIM	0.29962E 02	0.50816E 02
% DIF	0.74986E 00	0.73744E 00

ISOTOPE 240

	SIG-F	SIG-A
VIM	0.12923E 00	0.19018E 02
BGIM	0.12866E 00	0.18880E 02
% DIF	-0.44107E 00	-0.72563E 00

REACTIVITY ANALYSIS

	KIN-F
VIM	0.98182E 00
BGIM	0.98255E 00
% DELTA RHO	0.75707E-01

TABLE 39 HETERO CELL FUEL TYPE 8 LATTICE TYPE 6

MACROSCOPIC GROUP CONSTANTS

	NU SIG-F	SIG-A	SIG-R
VIM	0.60644E-01	0.75451E-01	0.49487E-01
BGIM	0.61617E-01	0.76060E-01	0.48471E-01
% DIF	0.16044E 01	0.80712E 00	-0.20531E 01

MICROSCOPIC GROUP CONSTANTS

ISOTOPE 238

	SIG-F	SIG-A
VIM	0.20881E-07	0.31672E 01
BGIM	0.21105E-07	0.31800E 01
% DIF	0.10727E 01	0.40415E 00

ISOTOPE 239

	SIG-F	SIG-A
VIM	0.29993E 02	0.50875E 02
BGIM	0.30475E 02	0.51676E 02
% DIF	0.16071E 01	0.15744E 01

ISOTOPE 240

	SIG-F	SIG-A
VIM	0.12481E 00	0.18245E 02
BGIM	0.12377E 00	0.17975E 02
% DIF	-0.83325E 00	-0.14798E 01

REACTIVITY ANALYSIS

	KIN-F
VIM	0.97815E 00
BGIM	0.97949E 00
% DELTA RHO	0.14046E 00

TABLE 40 HETERO CELL FUEL TYPE 1 LATTICE TYPE 1

MACROSCOPIC GROUP CONSTANTS

	NU SIG-F	SIG-A	SIG-R
VIM	0.52622E-01	0.65910E-01	0.73233E-01
BGIM	0.54158E-01	0.66739E-01	0.73083E-01
% DIF	0.29189E 01	0.12578E 01	-0.20466E 00

MICROSCOPIC GROUP CONSTANTS

ISOTOPE 238

	SIG-F	SIG-A
VIM	0.21739E-07	0.30504E 01
BGIM	0.21658E-07	0.30382E 01
% DIF	-0.37261E 00	-0.39993E 00

ISOTOPE 239

	SIG-F	SIG-A
VIM	0.30169E 02	0.50560E 02
BGIM	0.31049E 02	0.52157E 02
% DIF	0.29169E 01	0.31586E 01

REACTIVITY ANALYSIS

	KIN-F
VIM	0.12571E 01
BGIM	0.12589E 01
% DELTA RHO	0.11811E 00

TABLE 41 HETERO CELL FUEL TYPE 3 LATTICE TYPE 1

MACROSCOPIC GROUP CONSTANTS

	NU SIG-F	SIG-A	SIG-R
VIM	0.72231E-01	0.76090E-01	0.72240E-01
BGIM	0.70223E-01	0.75026E-01	0.73703E-01
% DIF	-0.27800E 01	-0.13983E 01	0.20252E 01

MICROSCOPIC GROUP CONSTANTS

ISOTOPE 238

	SIG-F	SIG-A
VIM	0.21379E-07	0.31221E 01
BGIM	0.21658E-07	0.30382E 01
% DIF	0.13050E 01	-0.26873E 01

ISOTOPE 239

	SIG-F	SIG-A
VIM	0.27445E 02	0.45360E 02
BGIM	0.26682E 02	0.44079E 02
% DIF	-0.27801E 01	-0.28241E 01

REACTIVITY ANALYSIS

	KIN-F
VIM	0.13303E 01
BGIM	0.13307E 01
% DELTA RHO	0.25213E-01

computer time used by a nuclear fuel cycle designer.

An exact comparison of computer times required by industry codes is very difficult due to differences in the problems calculated and the computers for which these codes are written. The simple problems reported in this study required the following CPU times on the IBM 370/165 computer at VPI&SU:

1. VIM - 4 hr.
2. BGIM (.00015 Integration step..003 Group Width) - 3 min.
3. EPRI - LEOPARD - 3 min.
4. MBGIM - 15 sec.

3.7. Analysis of Escape Probabilities

This section considers the accuracy of calculated escape probabilities and the sensitivity of resonance energy region cross sections and core neutron multiplication.

The first effect studied is the sensitivity of the macroscopic absorption cross section (energy range - 1.855 - 167 ev) and the infinite neutron multiplication factor to percentage changes in the escape probability from the fuel. This analysis is performed using the BGIM code to calculate fuel type 2 in lattice type 1. The calculated value of P_f is lowered or raised by the given percentage in the function subroutine that calculates P_f. The results of the altered BGIM calculation are then compared with the original to determine the effect of differences in P_f. The results for a series of these calculations are given in Table 42.

Table 42. Effect of Percentage Changes in P_f

% Change in P_f*	% Diff. in Σ_a*	% Diff. in Reactivity**
1	.4	-.08
-1	-.4	+.08
5	2.1	-.4
-5	-2.2	+.4
10	4.2	-.8
-10	-4.4	+.8

* A positive sign indicates that the altered value is higher

** % Dif. in reactivity is defined as

$$\frac{K_{\infty}^{Altered} - K_{\infty}^{Original}}{K_{\infty}^{Altered}\ K_{\infty}^{Original}} \times 100$$

The results show that differences in Σ_a and K_∞ are directly proportional to differences in P_f. The differences in K_∞ and Σ_a give a good indication of the accuracy in the calculation of P_f that is desired. P_f should be required to be accurate to within 5%. Ideally, P_f should be accurate to within 1-2%.

The next effect studied is the sensitivity of Σ_a and K_∞ to percentage changes in the moderator transmission probability (<Gm>). However, this time the results of the altered BGIM calculations of fuel type 2 in lattice type 1 are compared with the VIM results in Table 43. The base or original value of <Gm> is given by Sauer's formulation (20). The escape probability in all cases is calculated using Eq. (2.3.7) with Eq. (2.3.9) used for $<G_f>$.

The results in Table 43 indicate that the differences in Σ_a and K_∞ are also proportional to differences in <Gm> with a slightly greater sensitivity than is observed for changes in P_f. The results also indicate that at least for lattice type 1 the Sauer value for <Gm> used in Eq. (2.3.7) within the approximation of the BGIM theory is a good one. The results in section 3.5 comparing BGIM with VIM for a variety of lattice types also indicate that the <Gm> value given by Sauer's method is a good one. However, as is seen in the discussion of the effect of cladding on P_f, the best value of <Gm> is obtained by using it as a fitting parameter to Monte Carlo results.

Table 43. Effect of Percentage Changes in <Gm>

% Change in <Gm>*	% Diff. in Σ_a**	% Diff. in Reactivity**
1	-1.2	.1
-1	-.04	-.1
5	-3.8	.6
-5	2.3	-.6
10	-7.0	1.2

* A positive sign indicates that the altered value of <Gm> is greater than Sauer's.

** A positive sign indicates that the calculated value using the altered <Gm> is greater than VIM's.

*** % Diff. in reactivity is defined as

$$\frac{K_{\infty}^{\text{Altered}} - K_{\infty}^{\text{VIM}}}{K_{\infty}^{\text{Altered}}\, K_{\infty}^{\text{VIM}}} \times 100$$

It is instructive to compare values of P_f calculated using Eq. (2.3.9) with exact Monte Carlo values. Sauer's method is used for <Gm> and Eq. (2.3.7) is used for $<G_f>$ with A=0.1 and B=0. The results for a variety of lattice types and fuel cross sections are given in Tables 44-50.

These results show that the approximate methods for the calculation of P_f outlined in Section 2.3 give excellent agreement with the exact Monte Carlo results.

Next, the values for P_f using Eq. (2.3.7) and Eq. (2.3.9) are compared in Table 51 with those calculated using Eq. (2.3.7) and exact values for $<G_f>$.[24] These results indicate that Eq. (2.3.9) gives entirely adequate results. This is very important since Eq. (2.3.9) requires much less computation time than a tabular interpolation of exact results would.

The effect of cladding on the calculation of P_f is evaluated by performing two sets of Monte Carlo calculations. The first models a three region problem of fuel (varying $\Sigma_{T_{(f)}}$), cladding ($\Sigma_{T_{(c)}} = .777$), and moderator ($\Sigma_{T(m)} = 1.028$). The second models a two region problem of fuel (varying $\Sigma_{T_{(f)}}$) and moderator ($\Sigma_{T_{(m)}} = .9374$), where $\Sigma_{T_{(m)}}$ is the volume weighted average of $\Sigma_{T_{(c)}}$ and $\Sigma_{T_{(m)}}$ from the three region problem. These two sets of Monte Carlo calculations are compared in Table 52.

Table 44. Hexagonal Cell Escape Probabilities 1

$\Sigma_{t_{(m)}} = .9159$

Cell Pitch = .9144 cm

Pellet Radius = .3581 cm.

$\Sigma_{t_{(f)}}$	P_f VIM	P_f Eq. (2.3.7) & Eq. (2.3.9)
.698	.454 ± .003*	.458
1.396	.290 ± .004	.294
2.792	.164 ± .002	.169
4.188	.116 ± .002	.118
6.979	.070 ± .002	.073
13.959	.036 ± .002	.037

* The ± deviation is a one sigma (standard deviation) value obtained from a 20,000 neutron history Monte Carlo calculation.

Table 45. Hexagonal Cell Escape Probabilities 2

$\Sigma_{t_{(m)}} = .83368$

Cell Pitch = .8865 cm.

Pellet Radius = .3581 cm.

$\Sigma_{t_{(f)}}$	P_f VIM	P_f Eq. (2.3.7) & Eq. (2.3.9)
.698	.402 ± .004*	.409
1.396	.252 ± .004	.255
2.792	.142 ± .002	.144
4.188	.098 ± .002	.100
6.979	.059 ± .002	.061
13.959	.029 ± .001	.031

* The ± deviation is a one sigma value obtained from a 20,000 neutron history Monte Carlo.

Table 46. Hexagonal Cell Escape Probabilities 3

$\Sigma_{t_{(m)}} = 1.043$

Cell Pitch = .9783 cm.

Pellet Radius = .3581 cm.

$\Sigma_{t_{(f)}}$	$\bar{P}_f$ VIM	P_f Eq. (2.3.7) & Eq. (2.3.9)
.698	.529 ± .004*	.537
1.396	.360 ± .003	.362
2.792	.213 ± .003	.216
4.188	.150 ± .002	.153
6.979	.091 ± .002	.095
13.959	.047 ± .002	.048

* The ± deviation is a one sigma value obtained from a 20,000 neutron history Monte Carlo.

Table 47. Hexagonal Cell Escape Probabilities 4

$\Sigma_{t_{(m)}} = 1.227$

Cell Pitch = 1.1809 cm.

Pellet Radius = .3581 cm.

$\Sigma_{t_{(f)}}$	P_f VIM	P_f Eq. (2.3.7) & Eq. (2.3.9)
.698	.654 ± .003*	.655
1.396	.481 ± .003	.478
2.792	.304 ± .003	.304
4.188	.218 ± .003	.220
6.979	.136 ± .002	.139
13.959	.072 ± .002	.071

* The ± deviation is a one sigma value obtained from a 20,000 neutron history Monte Carlo.

Table 48. Hexagonal Cell Escape Probabilities 5

$\Sigma_{t_{(m)}} = .970$

Cell Pitch = 1.057 cm.

Pellet Radius = .419 cm.

$\Sigma_{t_{(f)}}$	P_f VIM	P_f Eq. (2.3.7) & Eq. (2.3.9)
.698	.444 ± .004	.450
1.396	.287 ± .003	.286
2.792	.162 ± .002	.163
4.188	.110 ± .003	.113
6.979	.066 ± .002	.070
13.959	.036 ± .001	.035

* The ± deviation is a one sigma value obtained from a 20,000 neutron history Monte Carlo.

Table 49. Square Cell Escape Probabilities 1

$\Sigma_{t_{(m)}} = 1.0$

Cell Pitch = 1.285

Pellet Radius = .419

$\Sigma_{t_{(f)}}$	P_f VIM	P_f Eq. (2.3.7) & Eq. (2.3.9)
.698	.610 ± .004*	.609
1.396	.429 ± .002	.429
2.792	.266 ± .002	.263
4.188	.186 ± .002	.187
6.979	.114 ± .002	.117
13.959	.057 ± .002	.059

* The ± deviation is a one sigma value obtained from a 20,000 neutron history Monte Carlo.

Table 50. Square Cell Escape Probabilities 2

$\Sigma_{t_{(m)}} = 1.0$

Cell Pitch = 1.080 cm.

Pellet Radius = .419 cm.

$\Sigma_{t_{(f)}}$	P_f VIM	P_f Eq. (2.3.7) & Eq. (2.3.9)
.698	.523 ± .003*	.521
1.396	.347 ± .003	.347
2.792	.205 ± .002	.204
4.188	.141 ± .002	.143
6.979	.085 ± .002	.088
13.959	.041 ± .001	.044

* The ± deviation is a one sigma value obtained from a 20,000 neutron history Monte Carlo.

Table 51. Lattice Escape Probability Comparison <Gm> = .6327

τ^*	P_f^1	P_f^2
.5	.457	.458
1.0	.294	.294
2.0	.169	.169
5.0	.0725	.0728
10.0	.0366	.0367

P_f^1 is obtained using Eq. (2.3.7) with exact values for $\langle G_f \rangle$.

P_f^2 is obtained using Eq. (2.3.7) with Eq. (2.3.9) used for $\langle G_f \rangle$.

τ^* equals $\Sigma_{t_{(f)}}$ X (Pellet Diameter)

The results in Table 52 indicate that volume weighting the clad and moderator gives reasonably good results, but there does exist a constant bias in the difference. This bias also exists when we use Sauer's method to obtain <Gm> in Eq. (2.3.7). Therefore, better results may be obtained by using <Gm> as a fitting parameter to make Eq. (2.3.7) agree with Monte Carlo results. This is illustrated in Table 53 for the three region problem given in Table 52.

Table 52. Comparison of P_f with Clad and with Clad/Mod Smear

Pitch = .9144 cm. (Hex. Cell)

Pellet Radius = .3581 cm.

Clad Radius = .4064 cm.

$\Sigma_{t_{(f)}}$	P_f^1	P_f^2
.698	.440 ± .003*	.454 ± .004
1.396	.282 ± .003	.291 ± .003
2.792	.165 ± .002	.169 ± .002
4.188	.113 ± .003	.118 ± .003
6.979	.068 ± .004	.072 ± .001
13.959	.032 ± .001	.034 ± .001

P_f^1 is calculated using three regions with $\Sigma_{t_{(m)}} = 1.028$ and $\Sigma_{t_{(c)}} = .777$.

P_f^2 is calculated using two region with $\Sigma_{t_{(m)}} = .937$

* The ± deviation is a one sigma value obtained from a 20,000 neutron history Monte Carlo.

Table 53. Comparison of P_f Calculated with Different <Gm>

τ	P_f^1	P_f^2	P_f VIM
.5	.462	.444	.440 ± .003 *
1	.298	.282	.282 ± .003
2	.172	.162	.165 ± .002
3	.120	.109	.113 ± .003
5	.074	.069	.068 ± .004
10	.037	.035	.032 ± .001

P_f^1 is calculated using Eq. (2.3.7) with Sauer's method used to determine <Gm>

P_f^2 is calculated using Eq. (2.3.7) with <Gm> chosen to make P_f agree with the Monte Carlo result for τ equal to 1.

* The ± deviation is a one-sigma value obtained from a 20,000 neutron history Monte Carlo.

4. CONCLUSIONS AND RECOMMENDATIONS

1. The results of this study show the "Broad Group Integral Method" (BGIM) is an efficient and accurate method for the calculation of neutron-nuclei reaction rates in the lower resolved resonance region. Almost all results from BGIM are within the statistical errors of the VIM calculations, which are typically 2-3% for the macroscopic group constants $\nu\Sigma_f$, Σ_a, and Σ_r, averaged over the energy range 1.855 ev - 167 ev. These results are very good compared to the differences with VIM obtained from MUFT-type codes, which approach 20% for group cross sectional values for tight lattices.[14] The additional accuracy obtained using the BGIM theory is obtained with little increased costs. It is estimated that for a 10-step unit cell fuel cycle depletion calculation, the computing time for a code such as EPRI-LEOPARD would be increased by only 6% if its lower resolved resonance region (1.855 ev - 167 ev) calculation is replaced by the more intricate BGIM method.

2. The Bell approximation, Eq. (2.3.7), adequately calculates the escape probability from a fuel rod that is part of a lattice when the correct transmission probabilities for fuel and moderator are used. For a three region problem of fuel, clad, and moderator, P_f calculated using Eq. (2.3.7) shows a maximum difference of 0.004 compared to mean values obtained from a 20,000 neutron history Monte Carlo calculation with a typical standard deviation of 0.003.

3. The extension of Chao's method for isolated rods, presented in this dissertation, provides a very accurate and fast calculation of the fuel transmission probability. Very little accuracy is gained over this method (<.001) when the exact value of the fuel transmission probability is used, which would require significant additional computational time.

4. A single energy independent moderator transmission probability is sufficient for use in Eq. (2.3.7). The moderator transmission probability is best defined as a fitting parameter that makes Eq. (2.3.7) agree with a Monte Carlo calculation of the escape probability for a rod that is part of a lattice.

5. A detailed energy solution of the transport equation is necessary to properly treat the complex effects of resonance overlap and interference. The spatial solution, even for tight lattices, is adequately treated using escape probabilities in a two region problem.

6. The use of BGIM together with a MUFT-type code is an excellent method which should be used for tight lattice unit cell calculations in order to obtain acceptable accuracy. This method could also be used to substantially improve the accuracy of current lightwater reactor loose lattice calculations. This is particularly true if the designer is interested in the calculation of isotopics in a nuclear fuel cycle depletion calculation since the calculation of isotopics requires more accurate resonance cross sections than the calculation of neutron multiplication. The small extra

computer cost, associated with the use of BGIM, is a good tradeoff for the increased accuracy obtained.

7. It is recommended that further work be done on the effect of cladding on the escape probability from a fuel rod that is part of a lattice. It is also recommended that a generalized method for determining the transmission probability through the moderator be investigated. This method should include the effects of cladding and should give accurate results for the fuel escape probability when used in Eq. (2.3.7).

8. It is recommended that the BGIM Theory be coded into a production computer program. This could be done in a stand-alone code, but it would most appropriately be programmed as a subroutine used in the lower resolved resonance energy region in a MUFT-type production code.

REFERENCES

1. EDLUND, M. C., "High Conversion Ratio Plutonium Recycle in Pressurized Water Reactors," Annals of Nuclear Energy, Vol. 2, pp. 801-807, Pergammon Press (1975).

2. WITTKOPF, W. A., et al., "NULIF - A Neutron Spectrum Generator, Few-Group Constant Calculator, and Fuel Depletion Code, BAW-10115A, Babcock and Wilcox, Lynchburg, Virginia (1977).

3. GAVIN, P. H. and RICKARD, I. C., "Performance of the Combustion Engineering PWR Physics Design System," Combustion Engineering Publication (1975).

4. PRAEL, R. E. and MILTON, L. J., "A User's Manual for the Monte Carlo Code, VIM," FRA-TM-84, Argonne National Laboratory (1976).

5. KIER, P. H. and ROBBA, A. A., "RABBLE, A Program for Computation of Resonance Absorption in Multiregion Reactor Cells," ANL-7326, Argonne National Laboratory (1967).

6. BOHL, H. and HEMPHILL, A. P., "MUFT-5, A Fast Neutron Spectrum Program for the Philco-2000," WAPD-TM-218, Bettis Atomic Power Laboratory (1961).

7. GOLDSTEIN, R., "An Equivalence Formulation for Absorption in Plutonium," Trans. Am. Nucl. Soc., 15:296(1972).

8. STRAWBRIDGE, L. E. and BARRY, R. F., "Criticality Calculations for Uniform Water-Moderated Lattices," Nucl. Sci. Eng., 23:58 (1965).

9. NORDHEIM, L. W., "A Program of Research and Calculations of Resonance Absorption," GA-2527, General Atomics (1961).

10. HELHOLTZ, J. and ROY, D. H., "STRIP - Resonance Absorption Program Treating Overlap and Interference," TP-332, Babcock and Wilcox, Lynchburg, Virginia (1967).

11. LEVITT, L. B. and LEWIS, R. C., "VIM-1, A Non multigroup Monte Carlo Code for Analysis of Fast Critical Assemblies," AI-AEC-12951, Atomics International (1970).

12. COHEN, M. O., "SAM-CE: A Three-Dimensional Monte Carlo Code for Foward Neutron and Foward and Adjoint Gamma Ray Transport Equations," MR-7021, Mathematical Applications Group, Inc. (1971).

13. LEVITT, L. B., "The Probability Table Method for Treating Unresolved Resonances in Monte Carlo Criticality Calculations," Trans. Am. Nucl. Soc., 14: [illegible](1971).

14. EDLUND, M. C. and SCHWENK, G. A., "Comparison of Results of Monte Carlo and CEPAC Calculations for Alternative Fuel Cycles," Virginia Polytechnic Institute and State University, Blacksburg, Virginia (1978).

15. HENRY, A. F., Nuclear Reactor Analysis, MIT Press, Cambridge, Massachusetts (1975).

16. KIRBY, K. D. and KARAM, R. A., "A General Method for Generating Effective Resonance Cross Sections for Heterogeneous Media," Nucl. Sci. Eng., 59:2;5 (1976).

17. BELL, G. I. and GLASSTONE, S., Nuclear Reactor Theory, Van Nostrand-Reinhold, New York (1970).

18. BARRY, R. F., "LEOPARD - A Spectrum Dependent Non-Spatial Depletion Code," WCAP-3269-26, Westinghouse Electric Corporation (1963).

19. CHAO, Y. A. and MARTINEZ, A. S., "On Approximations to the Neutron Escape Probability from an Absorbing Body," Nucl. Sci. Eng., 66: 254 (1978).

20. SAUER, A., "Approximate Escape Probabilities," Nucl. Sci. Eng., 16:329 (1963).

21. GELBARD, E. M. and SPANIER, J., Monte Carlo Principles and Neutron Transport Problems, Addison-Wesley, Reading, Mass. (1969).

22. PRAEL, R. E., "Cross Section Preparation for the Continuous-Energy Monte Carlo Code VIM," Nuclear Cross Sections and Technology, p. 447 (1975).

23. PRAEL, R. E. and HENRYSON, H., "A Comparison of VIM and MC^2-2 - Two Detailed Solutions of the Neutron Slowing Down Problem, "Nuclear Cross Sections and Technology, p. 451(1975).

24. CASE, K. M., et al., "Introduction to the Theory of Neutron Diffusion," Los Alamos Scientific Laboratory, Los Alamos, New Mexico (1953).

25. CHERNICK, J. and VERNON, R., "Some Refinements in the Calculation of Resonance Integrals," Nucl. Sci. Eng., 4:649 (1953).

26. EILAND, H.M., et al., "Epithermal Measurements of Capture and Fission Resonance Integrals in ^{235}U, ^{233}U, ^{239}Pu and ^{241}Pu," Nucl. Sci. Eng., 44:180 (1971).

27. HARDY, J., et al., "Influence of Molecular Binding Effects in Water on Measured Resonance Integrals," Nucl. Sci. Eng., 27:135 (1967).

28. HENRYSON, H., et al., "MC^2-2 A Code to Calculate Fast Neutron Spectra and Multigroup Cross Sections," ANL-8144, Argonne National Laboratory (1967).

29. THOMSEN, D. H. and TRAVER, T. M., "BMC-1: THE BATTELLE MONTE CARLO CODE," BMWL-1433, Battelle Northwest, June 1970.

APPENDIX A

GLOSSARY OF SYMBOLS
(Not defined in Text)

$J(\bar{r},e)$ ≡ neutron current as a function of space and energy.

Σ_t ≡ macroscopic total cross section

$\Sigma_S(E' \rightarrow E)$ ≡ the probability per unit path length that a neutron will scatter from E' to E.

ϕ ≡ the neutron flux.

$\bar{n}$ ≡ unit vector normal to a surface.

A_j ≡ Atomic weight of isotope j.

Σ_f ≡ macroscopic fission cross section.

Σ_a ≡ macroscopic absorption cross section.

Σ_r ≡ macroscopic removal cross section.

ν ≡ Average number of neutrons produced per fission.

```
C
C
C            ******** BGIM **********
C
C   BGIM SOLVES THE ENERGY DEPENDENT BOLTZMANN EQUATION IN THE RESOLVED
C RESONANCE ENERGY REGION USING THE THEORY DEVELOPED IN CHAPTER 2 OF THE
C REFERENCE.THE MAJOR OPTIONS IN BGIM ARE:
C
C      1.  CHOICE OF SIMPSON'S RULE INTEGRATION STEP SIZE
C      2.  CHOICE OF MULTIGROUP LETHARGY WIDTH
C      3.  CHOICE OF ENERGY RANGE OF SOLUTION,WHICH MUST BE BELOW 300 EV. AND
C          AND ABOVE 1.355 EV.
C      4.  CHOICE OF PERFORMING A HETEROGENEOUS OR HOMOGENEOUS SOLUTION
C      5.  CHOICE OF THE CALCULATION OF THE MULTIGROUP PARAMETERS.THEY MAY
C          BE CALCULATED DIRECTLY FROM THE VIM CROSS SECTION FILE USING THE
C          WORK SUBROUTINE,OR THEY MAY BE READ BY DINPUT FROM A PREVIOUSLY
C          WORK-RITE CREATED DISK FILE
C
C
C REFERENCE:  SCHWENK,G.A.,AN EFFICIENT METHOD FOR THE SOLUTION OF THE
C             ENERGY DEPENDENT INTEGRAL BOLTZMANN EQUATION IN THE RESOLVED
C             RESONANCE ENERGY REGION,PH.D DTSSERTATION,VPI&SU,MARCH,1980.
C
C               ******************************************
      COMMON/OPT/NOPT2,NOPT3
      COMMON/AB/NISO,NOPT1
      READ(5,1) NISO,NOPT2,NOPT3
      CALL RINPUT
      IF(NOPT2) 2,3,3
 2    CALL DINPUT
      GO TO 4
 3    CALL WORK
 4    CALL SOURCE
      IF(NOPT3) 5,6,6
```

```
 5     CALL RITE
 6     CONTINUE
       CALL SOLVE
       CALL EDIT
 1     FORMAT(12I6)
       STOP
       END
       SUBROUTINE RINPUT
C
C                **********  RINPUT ********
C
C    THIS SUBROUTINE READS PUNCHED CARD INPUT WHICH CONTAINS DATA SUCH AS
C    NUMBER DENSITIES AND OPTION DESIGNATORS.IT ALSO READS A TAPE FILE OF
C    VIM MICROSCOPIC POINTWISE CROSS SECTIONS.
C
C                ******************************************
      COMMON/OPT/NOPT2,NOPT3
      COMMON/AB/NISO,NOPT1
      COMMON PHO(3),NSTEP,ETOP,USPACE,PHOH,PHOOF,PHOOM,A,B,C,D
      COMMON/BB/NPTS(3),SIGP(3),NFILE(3)
     +,NGP(3),SIGSF(3),SIGFF(3),SIGAF(3),SIGTOF(3)
      COMMON/XSECT/SIGT(3,5120),SIGS(3,5120),SIGF(3,5120),EG
     +RID(3,5120)
      COMMON/CC/RLF,RLM,NBGRP,GAMMA,TSPACE,LABEL(3),VFM
     +,SIGPH,SIGPO,QXS,UT
      COMMON/DD/SOH,SUMOF,SUMOM,SUMF(3),ALPHA(3),ALPHAO,FIN1,FIN2
     +,P0(2,2300),P1(2,2300),P2(2,2300)
      READ(5,3) ITITL
      READ(5,1) NOPT1,NBGRP
      READ(5,2) A,B,C,D,RLF,RLM
      READ(5,2) PHOH,PHOOF,PHOOM,FIN1,FIN2,QXS
      READ(5,2) ETOP,USPACE,TSPACE,GAMMA,VFM,UT
      DO 5 I=1,NISO
      READ(5,1) NPTS(I),NFILE(I),NGP(I),LABEL(I)
```

```
      READ(5,2) PHO(I),SIGP(I),ALPHA(I)
5     CONTINUE
      DSPACE=TSPACE/2.
      WRITE(6,4) ITITL
      WRITE(6,13)
      WRITE(6,6)
      WRITE(6,7) NBGRP,ETOP,USPACE,DSPACE
      WRITE(6,8)
      WRITE(6,7) NOPT1,GAMMA
      WRITE(6,9)
      WRITE(6,14) RLF,RLM,VFM
      WRITE(6,11)
      WRITE(6,14) FIN1,FIN2,QXS
      WRITE(6,15)
      WRITE(6,14) PHOH,PHOOM,PHOOF
      WRITE(6,12)
      DO 30 I=1,NISO
      WRITE(6,7) LABEL(I),PHO(I),SIGP(I),ALPHA(I)
30    CONTINUE
      IF(NOPT2.LT.0)GO TO 20
      DO 10 I=1,NISO
      LUN=NFILE(I)
      NP=NPTS(I)
      READ(LUN) (EGRID(I,N),N=1,NP)
      READ(LUN) (SIGT(I,N),N=1,NP)
      READ(LUN) (SIGS(I,N),N=1,NP)
      READ(LUN) (SIGF(I,N),N=1,NP)
      REWIND  LUN
10    CONTINUE
20    CONTINUE
1     FORMAT(12I6)
2     FORMAT(6E12.6)
3     FORMAT(A80)
4     FORMAT('1',10X,A80)
```

```
 13   FORMAT('0',40X,10HINPUT DATA)
 6    FORMAT(10X,'NUMBER OF U GROUPS          ETOP',6X,
     +'GROUP LETHARGY WIDTH  INTEGRATION WIDTH')
 7    FORMAT(16X,I6,12X,3(E12.6,6X))
 8    FORMAT('0',10X,'      NOPT1                GAMMA')
   9  FORMAT('0',10X,'   MEAN CHORD FUEL     MEAN CHORD MOD',
     +'   FUEL TO MOD RATIO')
 14   FORMAT(16X,4(E12.6,6X))
 11   FORMAT('0',20X,'FIN1              FIN2              QXS')
 12   FORMAT('0',10X,'      ISOTOPE                PHO',
     +'                SIGP              ALPHA')
 15   FORMAT('0',10X,9X,'PHOH              PHOOM              PHOOF')
      RETURN
      END
      SUBROUTINE WORK
C
C                      *******  WORK *******
C
C      THIS SUBROUTINE USES A SIMPSON@S RULE INTEGRATION TO OBTAIN THE
C      INTEGRAL MULTIGROUP PARAMETERS,WHICH ARE NEEDED TO SOLVE EQ%2.2.30<
C      OF THE REFERENCE.%LINEAR INTERPOLATION OF THE VIM POINTWISE CROSS
C      SECTION FILE IS USED TO OBTAIN A CONTINUOUS CROSS SECTION DESCRIPTION
C      IN ENERGY.THUS,THE CHOICE OF INTEGRATION STEP SIZE AND MULTIGROUP
C      LETHARGY WIDTH ARE ARBITRARY.
C
C                      ****************************
C
      COMMON/AB/NISO,NOPT1
      COMMON PHO(3),NSTEP,ETOP,USPACE,PHOH,PHOOF,PHOOM,A,B,C,D
      COMMON/BB/NPTS(3),SIGP(3),NFILE(3)
     +,NGP(3),SIGSF(3),SIGFF(3),SIGAF(3),SIGTOF(3)
      COMMON/XSECT/SIGT(3,5120),SIGS(3,5120),SIGF(3,5120),EG
     +RID(3,5120)
      COMMON/CC/RLF,RLM,NBGRP,GAMMA,TSPACE,LABEL(3),VFM
```

```
     +,SIGPH,SIGPO,QXS,UT
      COMMON/DD/SOH,SUMOF,SUMOM,SUMF(3),ALPHA(3),ALPHAO,FIN1,FIN2
     +,P0(2,2300),P1(2,2300),P2(2,2300)
      REAL SIGTN(3,5120),RK(3,5120),SIGAN(3,5120),SIGFN(3,5120)
      REAL SS(35)
      EQUIVALENCE(SIGT,SIGTN),(EGRID,RK),(SIGS,SIGAN),(SIGF,SIGFN)
      DATA SIGPO/3.75/,SIGPH/20.45/,ALPHAO/.77855/
      SIGTM=PHOH*SIGPH+PHOOM*SIGPO
      TAUM=SIGTM*RLM
      GM=EXP(-TAUM)*(1.+C*TAUM*TAUM-D*TAUM*TAUM*TAUM)
      GM=.7121
      WRITE(6,2) GM
    2 FORMAT('0',10X,'GM=',F5.3)
      SIGPF=SIGPO*PHOOF
      DO 40 I=1,NISO
      SIGPF=SIGPF+PHO(I)*SIGP(I)
   40 CONTINUE
      U=ALOG(1.E+7/ETOP)
      DO 50 N=1,NBGRP
      EBGT=EXP(-U)*1.E+7
      EBGB=EXP(-(U+USPACE))*1.E+7
      ESPACE=EBGT-EBGT*EXP(-TSPACE)
      RESP=ESPACE/2.
      NSTEP=(EBGT-EBGB)/ESPACE
      NSTEP=NSTEP*2
      RN=FLOAT(NSTEP)
      DO 1 K=1,35
      SS(K)=0.0
    1 CONTINUE
      M=1
      NSTEP1=NSTEP+1
      DO 51 J=1,NSTEP1
      J1=J-1
      SIGTF=PHOOF*SIGPO+PHOH*SIGPH*NOPT1
```

```
      E=EBGT-J1*RESP
      DO 52 I=1,NISO
 60   IF(E.LT.EGRID(I,NGP(I)+1))NGP(I)=NGP(I)+1
      IF(E.LT.EGRID(I,NGP(I)+1))GO TO 60
      E1=EGRID(I,NGP(I))
      E2=EGRID(I,NGP(I)+1)
      SIGT1=SIGT(I,NGP(I))
      SIGT2=SIGT(I,NGP(I)+1)
      CALL INTERP(SIGT1,SIGT2,E1,E2,E,SIGTOF(I))
      SIGTF=SIGTOF(I)*PHO(I)+SIGTF
      SIGS1=SIGS(I,NGP(I))
      SIGS2=SIGS(I,NGP(I)+1)
      CALL INTERP(SIGS1,SIGS2,E1,E2,E,SIGSF(I))
      SIGF1=SIGF(I,NGP(I))
      SIGF2=SIGF(I,NGP(I)+1)
      CALL INTERP(SIGF1,SIGF2,E1,E2,E,SIGFF(I))
      SIGAF(I)=SIGTOF(I)-SIGSF(I)
 52   CONTINUE
      PF=PPF(A,B,SIGTF,RLF,GM,GAMMA)
      PM=PF*VFM*SIGTF/SIGTM
      EX1=E/1.E+7
      EX2=EX1*EX1
      PF1=PF*EX1
      PF2=PF*EX2
      PM1=PM*EX1
      PM2=PM*EX2
      FLX=FL(SIGTF,PF,SIGPF,GAMMA)
      FLX=FLX/E
      IF(J.EQ.NSTEP+1)M=1
      SS(1)=SS(1)+FLX*M
      SS(30)=SS(30)+PF*M
      SS(31)=SS(31)+PF1*M
      SS(32)=SS(32)+PF2*M
      SS(33)=SS(33)+PM*M
```

```
      SS(34)=SS(34)+PM1*M
      SS(35)=SS(35)+PM2*M
      DO 53 I=1,NISO
      SS(I+1)=SS(I+1)+FLX*SIGSF(I)*M*1.E+7/E
      I1=NISO+1+I
      SS(I1)=SS(I1)+FLX*SIGFF(I)*M
      I2=2*NISO+1+I
      SS(I2)=SS(I2)+FLX*SIGAF(I)*M
      I3=3*NISO+1+I
      SS(I3)=SS(I3)+FLX*SIGTOF(I)*M
53    CONTINUE
      M=M+2
      IF(M.NE.4)M=2
51    CONTINUE
      DO 54 I=1,NISO
      RK(1,N)=SS(I+1)/SS(1)
      I1=NISO+1+I
      I2=2*NISO+1+I
      SIGFN(I,N)=SS(I1)/SS(1)
      SIGAN(I,N)=SS(I2)/SS(1)
      I3=3*NISO+1+I
      SIGTN(I,N)=SS(I3)/SS(1)
54    CONTINUE
      H=USPACE/(RN*3.)
      P0(1,N)=SS(30)*H
      P1(1,N)=SS(31)*H
      P2(1,N)=SS(32)*H
      P0(2,N)=SS(33)*H
      P1(2,N)=SS(34)*H
      P2(2,N)=SS(35)*H
      U=U+USPACE
50    CONTINUE
      RETURN
      END
```

```
      SUBROUTINE SOURCE
C
C                        *****  SOURCE *******
C
C
C     THIS SUBROUTINE CALCULATES THE INTIAL HYDROGEN SOURCE AND THE STARTING
C     VALUES FOR SUM.
C
C                       **********************
C
      COMMON/AB/NISO,NOPT1
      COMMON PHO(3),NSTEP,ETOP,USPACE,PHOH,PHOOF,PHOOM,A,B,C,D
      COMMON/BB/NPTS(3),SIGP(3),NFILE(3)
     +,NGP(3),SIGSF(3),SIGFF(3),SIGAF(3),SIGTOF(3)
      COMMON/XSECT/SIGT(3,5120),SIGS(3,5120),SIGF(3,5120),EG
     +RID(3,5120)
      COMMON/CC/RLF,RLM,NBGRP,GAMMA,TSPACE,LABEL(3),VFM
     +,SIGPH,SIGPO,QXS,UT
      COMMON/DD/SOH,SUMOF,SUMOM,SUMF(3),ALPHA(3),ALPHAO,FIN1,FIN2
     +,P0(2,2300),P1(2,2300),P2(2,2300)
      REAL SIGTN(3,5120),RK(3,5120),SIGAN(3,5120),SIGFN(3,5120)
      EQUIVALENCE(SIGT,SIGTN),(EGRID,RK),(SIGS,SIGAN),(SIGF,SIGFN)
      SOH=USPACE*FIN2*PHOH*SIGPH
      LO=(.25033/USPACE)-1
      SUMKNO=SIGPO*EXP(UT-USPACE)*(1.-EXP(-LO*USPACE))/USPACE
      SUMOM=USPACE*FIN1*PHOOM*SUMKNO/(1.-ALPHAO)
      SUMOF=USPACE*FIN1*PHOOF*SUMKNO/(1.-ALPHAO)
      DO 10 I=1,NISO
      SUMF(I)=0.0
10    CONTINUE
      LJF=.0168/USPACE-1
      LJF1=LJF+1
      DO 20 I=1,NISO
      DO 30 N=2,LJF1
      SUMF(I)=SUMF(I)+RK(I,N)
```

```
 30   CONTINUE
      SUMF(I)=SUMF(I)*USPACE*QXS*PHO(I)/(1.-ALPHA(I))
 20   CONTINUE
      RETURN
      END
      SUBROUTINE RITE
C
C                     *****  RITE  ******
C
C     THIS SUBROUTINE WRITES OUT THE MULTIGROUP PARAMETERS CALCULATED BY
C     WORK TO A DISK FILE.
C
C                  ***************************
C
      COMMON/AB/NISO,NOPT1
      COMMON PHO(3),NSTEP,ETOP,USPACE,PHOH,PHOOF,PHOOM,A,B,C,D
      COMMON/BB/NPTS(3),SIGP(3),NFILE(3)
     +,NGP(3),SIGSF(3),SIGFF(3),SIGAF(3),SIGTOF(3)
      COMMON/XSECT/SIGT(3,5120),SIGS(3,5120),SIGF(3,5120),EG
     +RID(3,5120)
      COMMON/CC/RLF,RLM,NBGRP,GAMMA,TSPACE,LABEL(3),VFM
     +,SIGPH,SIGPO,QXS,UT
      COMMON/DD/SOH,SUMOF,SUMOM,SUMF(3),ALPHA(3),ALPHAO,FIN1,FIN2
     +,P0(2,2300),P1(2,2300),P2(2,2300)
      REAL SIGTN(3,5120),RK(3,5120),SIGAN(3,5120),SIGFN(3,5120)
      EQUIVALENCE(SIGT,SIGTN),(EGRID,RK),(SIGS,SIGAN),(SIGF,SIGFN)
      DO 10 N=1,NBGRP
      DO 20 I=1,NISO
      WRITE(3) SIGTN(I,N),SIGAN(I,N),SIGFN(I,N),RK(I,N)
 20   CONTINUE
      DO 30 J=1,2
      WRITE(3) P0(J,N),P1(J,N),P2(J,N)
 30   CONTINUE
 10   CONTINUE
```

```
     +,NGP(3),SIGSF(3),SIGFF(3),SIGAF(3),SIGTOF(3)
      COMMON/XSECT/SIGT(3,5120),SIGS(3,5120),SIGF(3,5120),EG
     +RID(3,5120)
      COMMON/CC/RLF,RLM,NBGRP,GAMMA,TSPACE,LABEL(3),VFM
     +,SIGPH,SIGPO,QXS,UT
      COMMON/DD/SOH,SUMOF,SUMOM,SUMF(3),ALPHA(3),ALPHAO,FIN1,FIN2
     +,P0(2,2300),P1(2,2300),P2(2,2300)
      REAL SIGTN(3,5120),RK(3,5120),SIGAN(3,5120),SIGFN(3,5120)
      REAL SS(35)
      EQUIVALENCE(SIGT,SIGTN),(EGRID,RK),(SIGS,SIGAN),(SIGF,SIGFN)
      COMMON/FF/FLUX(2,2300),LJS
      REAL UN(300),RRFI(3),RRAI(3),XSECA(3),XSECF(3),TOTAI(3),TOTFI(3)
      REAL OSIGA(3),OSIGF(3),RNU(3)
      DATA XSICH/20.5/,XSIGO/.44/,RNU(1)/2.32/,RNU(2)/2.873/
     +,RNU(3)/2.870/
      READ(5,1) NMGE
      READ(5,2) (UN(I),I=1,NMGE)
      WRITE(6,3)
      WRITE(6,4)
      L=LJS
      LS=(UN(1)-UT)/USPACE+L
      NMGE1=NMGE-1
      TFLIC=0.0
      DO 60 I=1,NISO
      TOTAI(I)=0.0
      TOTFI(I)=0.0
60    CONTINUE
      DO 10 NG=1,NMGE1
      FM1=0.0
      FFI=0.0
      DO 50 I=1,NISO
      RRFI(I)=0.0
      RRAI(I)=0.0
50    CONTINUE
```

```
      DO 20 N=L,LS
      FMI=FMI+FLUX(2,N)*USPACE
      FFI=FFI+ FLUX(1,N)*USPACE
      DO 30 I=1,NISO
      RRFI(I)=RRFI(I)+SIGFN(I,N)*FLUX(1,N)*USPACE
      RRAI(I)=RRAI(I)+SIGAN(I,N)*FLUX(1,N)*USPACE
30    CONTINUE
20    CONTINUE
      FLIC=FMI+VFM*FFI
      FLIC=FLIC/(1.+VFM)
      DO 40 I=1,NISO
      XSECA(I)=(1.+1./VFM)*RRAI(I)*VFM/(FMI+VFM*FFI)
      XSECF(I)=(1.+1./VFM)*RRFI(I)*VFM/(FMI+VFM*FFI)
      RRAI(I)=FLIC*PHO(I)*XSECA(I)/(1.+1./VFM)
      RRFI(I)=FLIC*PHO(I)*XSECF(I)/(1.+1./VFM)
      TOTAI(I)=TOTAI(I)+RRAI(I)
      TOTFI(I)=TOTFI(I)+RRFI(I)
      WRITE(6,5) UN(NG),FLIC,LABEL(I),XSECA(I),XSECF(I),RRAI(I),RRFI(I)
40    CONTINUE
      TFLIC=TFLIC+FLIC
      L=LS
      LS=LS+(UN(NG+1)-UN(NG))/USPACE
10    CONTINUE
      WRITE(6,6)
      HPO=PHOOM/(1.+VFM)+PHOOF/(1.+1./VFM)
      XS=XSIGO*HPO
      REM=FLIC*XS/TFLIC
      REM=REM/(UN(NG)-UN(NG-1))
      REM=REM+SOH/(USPACE*TFLIC*(1.+VFM*GAMMA))
      DO 70 I=1,NISO
      OSIGA(I)=(1.+1./VFM)*TOTAI(I)/(TFLIC*PHO(I))
      OSIGF(I)=(1.+1./VFM)*TOTFI(I)/(TFLIC*PHO(I))
      WRITE(6,7) LABEL(I),TOTAI(I),TOTFI(I),OSIGA(I),OSIGF(I),TFLIC
70    CONTINUE
```

```
      PRO=0.0
      ABS=0.0
      DO 80 I=1,NISO
      ABS=ABS+TOTAI(I)/TFLIC
      PRO=PRO+TOTFI(I)*RNU(I)/TFLIC
 80   CONTINUE
      WRITE(6,8)
      WRITE(6,9)
      WRITE(6,11)PRO,ABS,REM
 1    FORMAT(12I6)
 2    FORMAT(6E12.6)
 3    FORMAT('1',40X,16HCALCULATED DATA )
 4    FORMAT('0',10X,'  LETHARGY     FLUX          ISOTOPE     SIG-A ',
     +'       SIG-F    ABSORP RATE FISSION RATE')
 5    FORMAT('0',10X,2E12.5,I12,4E12.5)
 6    FORMAT(10X,'   ISOTOPE  ABSORP RATE I FISS RATE I',3X,
     +'SIG-A       SIG-F       FLUX I')
 7    FORMAT(13X,I6,3X,5E12.5)
 8    FORMAT('0',20X,'MACROSCOPIC GROUP CONSANTS')
 9    FORMAT('0',10X,'NU SIG-F              SIG-A               SIG-R')
 11   FORMAT(10X,3(E12.5,6X))
      RETURN
      END
      FUNCTION PPF(A,B,SIGTF,RLF,GM,GAMMA)
C
C                *******  PPF  ******
C
C     THIS IS A FUNCTION SUBROUTINE THAT CALCULATES ESCAPE PROBALITIES.
C
C                **********************
C
      TAU=SIGTF*RLF
      GF=EXP(-TAU)*(1.+A*TAU*TAU-B*TAU*TAU*TAU)
      PPF=(1.-GF)*(1.-GM)
```

```
      PPF=PPF/(TAU*(1.-GM*GF))
      PPF=PPF*GAMMA
      RETURN
      END
      FUNCTION FL(SIGTF,PF,SIGPF,GAMMA)
C
C                  *******  FL  ********
C
C     THIS IS A FUNCTION SUBROUTINE THAT CALCULATES THE NEUTRON FLUX SHAPE
C     IN ENERGY.
C
C                  ********************
C
      FL=(1.-GAMMA*PF)/SIGTF
      FL=FL+GAMMA*PF/SIGPF
      RETURN
      END
```

```
      RETURN
      END
      SUBROUTINE DINPUT
C                     ***** DINPUT ******
C
C     THIS SUBROUTINE READS THE DISK FILE CREATED BY RITE
C
C                     ********************
C
      COMMON/AB/NISO,NOPT1
      COMMON PHO(3),NSTEP,ETOP,USPACE,PHOH,PHOOF,PHOOM,A,B,C,D
      COMMON/BB/NPTS(3),SIGP(3),NFILE(3)
     +,NGP(3),SIGSF(3),SIGFF(3),SIGAF(3),SIGTOF(3)
      COMMON/XSECT/SIGT(3,5120),SIGS(3,5120),SIGF(3,5120),EG
     +RID(3,5120)
      COMMON/CC/RLF,RLM,NBGRP,GAMMA,TSPACE,LABEL(3),VFM
     +,SIGPH,SIGPO,QXS,UT
      COMMON/DD/SUH,SUMOF,SUMOM,SUMF(3),ALPHA(3),ALPHAO,FIN1,FIN2
     +,P0(2,2300),P1(2,2300),P2(2,2300)
      REAL SIGTN(3,5120),RK(3,5120),SIGAN(3,5120),SIGFN(3,5120)
      EQUIVALENCE(SIGT,SIGTN),(EGRID,RK),(SIGS,SIGAN),(SIGF,SIGFN)
      DO 10 N=1,NBGRP
      DO 20 I=1,NISO
      READ(3) SIGTN(I,N),SIGAN(I,N),SIGFN(I,N),RK(I,N)
 20   CONTINUE
      DO 30 J=1,2
      READ(3) P0(J,N),P1(J,N),P2(J,N)
 30   CONTINUE
 10   CONTINUE
      RETURN
      END
      SUBROUTINE INTERP(F1,F2,E1,E2,E,ANS)
C
C                  *******  INTERP  ******
```

```
C
C     THIS SUBROUTINE PERFORMS A LINEAR INTERPOLATION.
C
C                  **********************
C
      ANS=(E1-E)/(E1-E2)
      ANS=ANS*(F1-F2)+F1
      RETURN
      END
      SUBROUTINE SOLVE
C
C                     *******  SOLVE  ******
C
C     THIS SUBROUTINE USES A STEPPING UP IN LETHARGY PROCEDURE TO SOLVE
C     EQ.(2.2.30). IT ALSO USES THE RECURRENCE RELATIONSHIPS GIVEN IN
C     SECTION 2.5 OF THE REFERENCE TO CALCULATE SUM AND SH.
C
C                     **********************
C
      COMMON/AB/NISO,NOPT1
      COMMON PHO(3),NSTEP,ETOP,USPACE,PHOH,PHOOF,PHOOM,A,B,C,D
      COMMON/BB/NPTS(3),SIGP(3),NFILE(3)
     +,NGP(3),SIGSF(3),SIGFF(3),SIGAF(3),SIGTOF(3)
      COMMON/XSECT/SIGT(3,5120),SIGS(3,5120),SIGF(3,5120),EG
     +RID(3,5120)
      COMMON/CC/RLF,RLM,NBGRP,GAMMA,TSPACE,LABEL(3),VFM
     +,SIGPH,SIGPO,QXS,UT
      COMMON/DD/SOH,SUMOF,SUMOM,SUMF(3),ALPHA(3),ALPHAO,FIN1,FIN2
     +,PO(2,2300),P1(2,2300),P2(2,2300)
      REAL SIGTN(3,5120),RK(3,5120),SIGAN(3,5120),SIGFN(3,5120)
      REAL SS(35)
      EQUIVALENCE(SIGT,SIGTN),(EGRID,RK),(SIGS,SIGAN),(SIGF,SIGFN)
      COMMON/FF/FLUX(2,2300),LJS
      ARG=FLOAT(LABEL(1))
```

```
      ARG=(ARG+1.)/(ARG-1.)
      EJ=2.*ALOG(ARG)
      LJ=EJ/USPACE-1
      LJO=(.25033/USPACE)-1
      LJS=LJ+2
      UN1=UT
      UN=UT+USPACE
      SIGTMN=PHOM*SIGPH+PHOOM*SIGPO
      EUSP=EXP(-USPACE)
      LJ1=LJ+1
      DO 1 N=1,LJ1
      FLUX(1,N)=FIN1
      FLUX(2,N)=FIN1
    1 CONTINUE
      DO 10 N=LJS,NBGRP
      SIGTFN=0.
      DO 20 I=1,NISO
      SIGTFN=SIGTFN+PHO(I)*SIGIN(I,N)
   20 CONTINUE
      SIGTFN=SIGTFN+PHOOF*SIGPO+SIGPH*PHOM*NOPT1
      EXUN=EXP(UN)
      EXUN1=EXP(UN1)
      RKOMIC=SIGPO*(EXUN-EXUN1)/USPACE
      RKOMN=RKOMIC*PHOOM/(1.-ALPHAO)
      RKOFN=RKOMIC*PHOOF/(1.-ALPHAO)
      RKOMIC=SIGPO*(EXP(UN-(LJO+1)*USPACE)-EXP(UN1-(LJO+1)*USPACE))
      RKOMIC=RKOMIC/USPACE
      RKOMNL=RKOMIC*PHOOM/(1.-ALPHAO)
      RKOFNL=RKOMIC*PHOOF/(1.-ALPHAO)
      AL=1./EXUN1-1./EXUN
      BETA=(EXP(-2.*UN1)-EXP(-2.*UN))/2.
      NLO=N-LJO-1
      IF(NLO.LT.1)NLO=1
      IF(N.EQ.LJS)GO TO 5
```

```
      SUMOF=SUMOF-RKOFNL*FLUX(1,NLO)*USPACE+RKOFN1*FLUX(1,N-1)*USPACE
      SUMOM=SUMOM-RKOMNL*FLUX(2,NLO)*USPACE+RKOMN1*FLUX(2,N-1)*USPACE
5     CONTINUE
      TERM1=0.
      TERM2=0.
      TERM3=0.
      TERM4=0.
      DO 30 J=1,NISO
      TERM1=TERM1+(EUSP*EXUN*PHO(J)*RK(J,N-LJ-1)*FLUX(1,N-LJ-1)
     +*P2(1,N)/(1.-ALPHA(J))+SUMF(J)*P1(1,N)/USPACE)*(1-NOPT1)*VFM
      TERM2=TERM2+P0(1,N)*PHO(J)*RK(J,N)/((1.-ALPHA(J))*EXUN)
      TERM3=TERM3+PHO(J)*RK(J,N)*(USPACE-P0(1,N))/((1.-ALPHA(J))*EXUN)
      TERM4=TERM4+EUSP*EXUN*PHO(J)*RK(J,N-LJ-1)*FLUX(1,N-LJ-1)
     +*(BETA-P2(1,N))/(1.-ALPHA(J))+SUMF(J)*(AL-P1(1,N))/USPACE
30    CONTINUE
      SOHD=SOH/USPACE
      YEL=SIGTMN-(1./EXUN*RKOMN*(USPACE-P0(2,N)))
      PUR=EUSP*EXUN*RKOMNL*FLUX(2,NLO)*(BETA-P2(2,N))
      PUR=PUR+SUMOM*(AL-P1(2,N))/USPACE
      PUR=PUR+SOHD*(1.-P0(2,N)/USPACE)
      PUR=PUR+VFM*(EUSP*EXUN*RKOFNL*FLUX(1,NLO)*P2(1,N)+SUMOF*
     +P1(1,N)/USPACE)
      PUR=PUR+TERM1
      BLA=RKOFN*P0(1,N)/EXUN+TERM2
      BLA=BLA*VFM
      RED=SIGTFN-RKOFN*(USPACE-P0(1,N))/EXUN-TERM3
      BLU=EUSP*EXUN*RKOFNL*FLUX(1,NLO)
     +*(BETA-P2(1,N))+SUMOF*(AL-P1(1,N))/USPACE
      BLU=BLU+TERM4
      BLU=BLU+(EUSP*EXUN*RKOMNL*FLUX(2,NLO)*
     +P2(2,N)+SUMOM*P1(2,N)/USPACE)/VFM
      BLU=BLU+SOHD*P0(2,N)/(USPACE*VFM)+NOPT1*SOHD/USPACE
      CRO=RKOMN*P0(2,N)/(EXUN*VFM)
      FLUX(1,N)=(BLU+CRO*PUR/YEL)/(RED-CRO*BLA/YEL)
```

```
      FLUX(2,N)=PUR/YEL+BLA*FLUX(1,N)/YEL
      IF(NOPT1.EQ.1)FLUX(2,N)=FLUX(1,N)
      SUH=EUSP*SUH+USPACE*(1.-EUSP)*SIGPH*PHOH*FLUX(2,N)
      NTG=UN1/USPACE-1
      SUH=SUH-USPACE*(1.-EUSP)*SIGPH*FLUX(2,1)*EXP(-NTG*USPACE)*PHOH
      DO 40 J=1,NISO
      SUMF(J)=SUMF(J)-PHO(J)*RK(J,N-LJ)*FLUX(1,N-LJ)*USPACE/(1.-ALPHA(
     +J))+PHO(J)*RK(J,N)*FLUX(1,N)*USPACE/(1.-ALPHA(J))
 40   CONTINUE
      UN1=UN1+USPACE
      UN=UN+USPACE
      RKOMN1=RKOMN
      RKOFN1=RKOFN
 10   CONTINUE
      RETURN
      END
      SUBROUTINE EDIT
C
C                     ***** EDIT *****
C
C     THIS SUROUTINE PREFORMS THE OUTPUT EDITING,WHICH CONSISTS OF:
C
C       1.  MACROSCOPIC GROUP CONSTANTS NU-SIGF,SIG-A,SIG-R AND THE MICROSCOPIC
C           CROSS SECTIONS SIG-F AND SIG-A AVERAGED OVER THE ENERGY RANGE
C           OF SOLUTION.
C
C       2.  THE FLUX AND ABSORBTION AND FISSION RATES BY ISOTOPE INTEGRATED
C           OVER THE ENERGY RANGE OF SOLUTION.
C
C                  ******************************
C
      COMMON/AB/NISO,NOPT1
      COMMON PHO(3),NSTEP,ETOP,USPACE,PHOH,PHOOF,PHOOM,A,B,C,D
      COMMON/BB/NPTS(3),SIGP(3),NFILE(3)
```

The vita has been removed from the scanned document

AN EFFICIENT METHOD FOR THE SOLUTION OF THE ENERGY DEPENDENT INTEGRAL BOLTZMANN TRANSPORT EQUATION IN THE RESOLVED RESONANCE ENERGY REGION

by

George A. Schwenk, Jr.

(ABSTRACT)

The calculation of neutron-nuclei reaction rates in the lower resolved resonance region (167 ev - 1.855 ev) is considered in this dissertation. Particular emphasis is placed on the calculation of these reaction rates for tight lattices where their accuracy is most important. The results of the continuous energy Monte Carlo code, VIM, are chosen as reference values for this study.

The primary objective of this work is to develop a method for calculating resonance reaction rates which agrees well with the reference solution, yet is efficient enough to be used by nuclear reactor fuel cycle designers on a production basis. A very efficient multigroup solution of the two spatial region energy dependent integral transport equation is developed. This solution, denoted the "Broad Group Integral Method" (BGIM), uses escape probabilities to obtain the spatial coupling between regions and uses an analytical flux shape within a multigroup to obtain weighted

cross sections which account for the rapidly varying resonance cross sections. The multigroup lethargy widths chosen for the numerical integration of the two region energy-dependent neutron continuity equations can be chosen much wider (a factor of 30 larger) than in the direct numerical integration methods since the analytical flux shape is used to account for fine structure effects. The BGIM solution is made highly efficient through the use of these broad groups. It is estimated that for a 10 step unit cell fuel cycle depletion calculation, the computer running time for a production code such as EPRI-LEOPARD would be increased by only 6% through the use of the more accurate and intricate BGIM method in the lower resonance energy region.

A comprehensive numerical verification of the proposed method is performed. Numerous comparisons are made to VIM for an infinite repeating lattice. These comparisons consider isotopic changes caused by burnup and enrichment variations, cold and hot temperatures in fuel and moderator, and lattice geometry variations. These results show the "Broad Group Integral Method" (BGIM) to be an efficient and accurate solution of the energy dependent integral Boltzmann transport equation in the resolved resonance energy region.